Philosophical Magazine A

ISSN: 0141-8610 (Print) 1460-6992 (Online) Journal homepage: https://www.tandfonline.com/loi/tpha20

Misfit strain and misfit dislocations in lattice mismatched epitaxial layers and other systems

S. C. Jain , A. H. Harker & R. A. Cowley

To cite this article: S. C. Jain , A. H. Harker & R. A. Cowley (1997) Misfit strain and misfit dislocations in lattice mismatched epitaxial layers and other systems, Philosophical Magazine A, 75:6, 1461-1515, DOI: 10.1080/01418619708223740

To link to this article: https://doi.org/10.1080/01418619708223740

PHILOSOPHICAL MAGAZINE A, 1997, VOL. 75, No. 6, 1461–1515

Misfit strain and misfit dislocations in lattice mismatched epitaxial layers and other systems*

By S. C. JAIN†§, A. H. HARKER‡¶ and R. A. COWLEY†

† Clarendon Laboratory, University of Oxford, Oxford, UK
‡ Department of Materials, Imperial College, London, UK

[*Received 11 January 1996 and accepted 12 July 1996*]

ABSTRACT

Heterostructures in the form of thin layers of one material grown on a substrate have been the subject of intense study for several years. In the case of semiconductor systems the aim is to grow epitaxial layers of, for example, $Si_{1-x}Ge_x$ on Si, and devices based on such structures are already in use. Much is known, as is summarized in this review, about the stability of such systems against the insertion of dislocations, and about the critical thicknesses up to which strained layer structures are stable. The effects of dislocation nucleation and the dynamics of dislocation motion which lead to strain relaxation in metastable systems are also reviewed. The present state of theoretical understanding is compared with what is known experimentally.

For metallic systems, which often exhibit magnetic properties, the underlying problems of lattice mismatch and strain relief are similar, but much of the interest has been concentrated on the commensurate–incommensurate transition in both structurally and magnetically modulated materials. The theory of this transition is reviewed, both for metallic systems and for epitaxial layers on graphite.

In bringing together these different classes of systems within one review, it has been possible to demonstrate the parallels between them. It is hoped that, as a result, transfers of ideas between the fields will be promoted.

CONTENTS

	PAGE
1. Introduction	1462
1.1. Importance of strain in device technology	1462
1.2. Historical survey of strained layers and heterostructures	1464
2. Strain and dislocations	1466
2.1. Misfit strain	1466
2.2. Critical layer thickness h_c	1467
2.3. Misfit dislocations	1468
2.4. The energy of the dislocations	1468
2.4.1. Dislocations in epilayers with free surfaces	1468
2.4.2. Capped layers	1469
2.4.3. Energy of non-periodic arrays of dislocations	1471
2.4.4. Total energy of the strained layers containing dislocations	1472

*This paper was originally received and accepted for *Advances in Physics*, however, to better reflect the subject matter and to increase timeliness of publication, the Editors of *Advances in Physics* have decided to transfer the paper to *Philosophical Magazine* A.

§ Present address: IMEC, Kapeldreef 75, 3001 Leuven, Belgium.
¶ Present address: Centre for Materials Research, University College, London, UK.

3. Critical thickness 1475
3.1. Theories of the critical thickness h_c 1475
3.2. Experimental values of h_c 1477
4. Thick epilayers in equilibrium 1479
5. Motion of dislocations 1481
5.1. The glide velocity 1481
5.1.1. The double kink model 1482
5.1.2. The single kink model 1484
5.2. Experimental results 1484
6. Nucleation, multiplication and blocking 1486
6.1. Nucleation 1486
6.2. Multiplication 1489
6.3. Blocking 1490
7. Annealing and strain relaxation 1492
7.1. Excess stress and the Dodson–Tsao equation 1492
7.2. Improved theory of strain relaxation 1494
7.3. Interpretation of annealing experiments 1495
8. Metallic systems 1497
9. Structure of absorbed monolayers 1499
9.1. Commensurate–incommensurate transitions 1499
9.2. Two-dimensional melting 1502
9.3. Rotational epitaxy 1502
10. Incommensurate structures 1503
10.1. Continuum theories of commensurate–incommensurate phase transitions 1503
10.2. Lattice models 1504
10.3. Experimental measurements 1506
11. Conclusions 1509
Acknowledgments 1511
References 1511

§ 1. Introduction

1.1. *Importance of strain in device technology*

Attention has been paid recently to the fabrication of lattice mismatched epitaxial layer (or simply epilayer) devices [1–5]. In the case of semiconductors this is due to the beneficial effect that the strain can have on the electronic properties of the layers. Layers grown on (100) Si or GaAs substrate are tetragonally distorted. The bandgap, effective masses of the holes and electrons, and the mobility are the parameters which determine the suitability of a semiconductor for a specific application, and the tetragonal strain modifies these parameters [5–8]. The distortion removes the degeneracy of the valence band. Under compression, the heavy hole band moves up and the light hole band moves down. The conduction band of cubic Ge_xSi_{1-x} alloys remains Si like for $x < 0{\cdot}8$ and the lowest band remains sixfold degenerate. In the strained layers, the sixfold degenerate conduction band splits into a fourfold degenerate valley which, under compression, decreases in energy while the twofold degenerate valley increases. Due to this band splitting and due to a small hydrostatic component of the strain, the bandgap $E_g(x, T)$ of Ge_xSi_{1-x} strained

Fig. 1

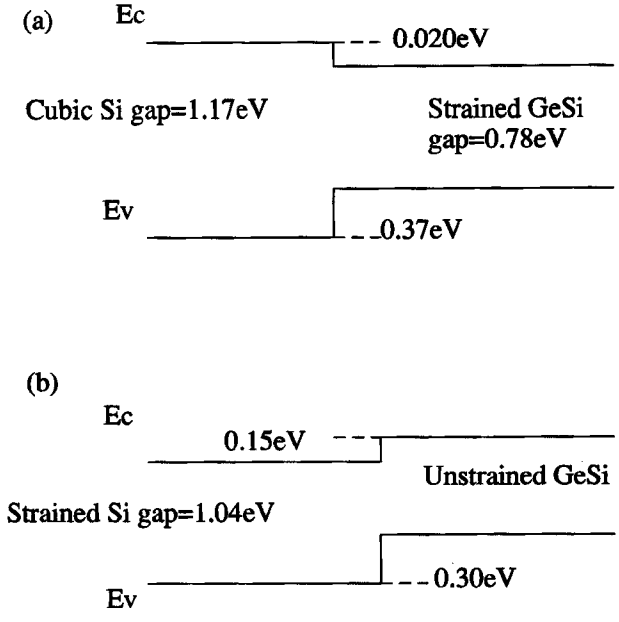

Band alignments for (*a*) $Ge_{0.2}Si_{0.8}$ on unstrained Si(100) substrate and (*b*) alternate layers of $Ge_{0.5}Si_{0.5}$ and Si on relaxed (unstrained) $Ge_{0.25}Si_{0.75}$(100) substrate [10].

layers decreases with x and is given by [9],

$$E_g(x, T) = E_g(0, T) - 0{\cdot}96x + 0{\cdot}43x^2 - 0{\cdot}17x^3, \tag{1}$$

where $E_g(0, T)$ is the bandgap of Si at temperature T. For $x = 0{\cdot}6$, $E_g = 0{\cdot}533$ eV at 300 K. Thus for 60% Ge in the strained alloy layer, its bandgap becomes smaller than the bandgap (0·666 eV) of unstrained Ge. The bandgap of strained Ge on a Si(100) substrate is only 0·42 eV. The advantages of these large changes in the bandgap energy are obvious. Strained layers absorb infrared radiation at longer wavelengths making them suitable for use as infrared (IR) detectors. The effective masses of both electrons and holes are modified by the strain, and the hole mobility increases due to the strain, improving the performance of almost all devices. The electron mobility perpendicular to the interface also increases which reduces the base transit time in n–p–n heterostructure bipolar transistors (HBTs).

More spectacular advantages arise from the discontinuities in the alignment of band edges at the heterojunction. As an example, the band alignments of two GeSi heterostructures are shown in figure 1. In case (*a*), the reduction in the band gap of a $Ge_{0.2}Si_{0.8}$ strained layer is 0·17 eV.† Most of this reduction is in the discontinuity of the valence band edge. In Ge_xSi_{1-x} layers under compression, the conduction band discontinuity containues to be small for all values of x. The valence band edge discontinuity always dominates the reduction. This valence band discontinuity is very useful in improving the performance of n–p–n HBTs. Heavy doping allows a reduction in the base thickness, reduces the base resistance, avoids punch through,

† This value is slightly smaller than that given by equation (1).

and reduces the base transit time. If a thin strained layer is sandwiched between two Si epitaxial layers, a p-type quantum well is formed. The depth of this well can be tailored by adjusting the strain which increases monotonically with x. Modulation doping and a two-dimensional hole gas are easily achieved [11]. High performance heterostructure bipolar transistors [12, 13], IR detectors for defence and space applications (8 to 18 μm range) [6, 14], p-channel metal–oxide–silicon field effect transistors (MOSFETs) with high transconductance [15], high mobility modulation doped field effect transistors (MODFETs) [4] and a host of other devices have been developed [1, 5, 9]. Strain provides another degree of freedom which can be used to adjust the band structure and electronic properties of a heterostructure and enables us to fabricate new devices or enhance the performance of existing devices.

Similar progress has been made in the applications of InGaAs strained layer heterostructure devices. Bandgaps, band-offsets and valence band structure have been calculated and measured [16, 17]. As a result significant advances have been made in the performance of InGaAs strained layer lasers and high speed MODFETs [18–21].

Short wavelength solid state lasers are important. They are needed for optical memory and printing applications. Much greater data densities could be put on an optical disc if short wavelength lasers were to become available [22]. The commercial implications of the development of short wavelength lasers are well known. For decades II–VI semiconductors, particularly ZnSe, have been considered as potential candidates for emitters of visible light. There have been two main difficulties in making them into diode light emitters in the visible range of the spectrum. It is difficult to dope these semiconductors both p and n type and hence to fabricate a p–n junction diode. Also, there was not a suitable pair of lattice matched II–VI semiconductors with different bandgaps for fabricating the required heterostructure. Using modern deposition techniques, p doping has been accomplished using Li or N as dopants [23] while Cl is used for n-type doping. A strained layer structure p-ZnSe/$Cd_{0.2}Zn_{0.8}Se$/n-ZnSe grown on GaAs substrate [24, 25] has turned out to be a suitable structure, so that strained layer technology has at long last enabled blue–green light emitting diodes (LEDs) and lasers to become a reality [25, 26].

Although most of the detailed work on strained heterostructures has been on semiconductors, metallic heterostructures are beginning to play an important role. Of particular technological interest is the discovery [27, 28] of the giant magneto-resistance effect which potentially will provide new magnetic sensors and improved magnetic read heads. The role of strain, surface roughness and interface strain on these devices is still unknown. Another application is the discovery [29] of the supermodulus effect in superlattices in which the elastic moduli are very different from those of the constituent materials. Again strain and lattice mismatch play an important part in determining the properties of these materials.

1.2. *Historical survey of strained layers and heterostructures*

Many years ago, Shockley suggested the use of semiconductors with zones having different bandgaps for the fabrication of semiconductor devices ([30], see also [31]). In the 1960s and 1970s, many attempts were made to grow a layer of one semiconductor (of a given bandgap) over another (with another bandgap). At that time the general tendency was to avoid strain because it was found that strain degraded the quality of the epitaxial layers and rendered them unsuitable for device fabrication. $Al_xGa_{1-x}As$ and GaAs are closely lattice matched for all values of x

Table 1. Room temperature lattice constants in angstroms and bandgaps in electronvolts of semiconductors commonly used for fabricating heterostructure devices.

Semiconductor	Lattice constant	Bandgap	Reference
AlP	5·4635	3·6(Γ)	[33]
	5·4635	3·5(L)[a]	[33]
AlAs	5·6605	2·15(X)	[33]
AlSb	6·1358	1·612(X)	[33]
GaP	5·4510	2·272(X)	[33]
GaAs	5·653 25	1·424(Γ)	[33]
GaSb	6·096 02	0·725(Γ)	[33]
InP	5·8689	1·350(Γ)	[33]
InAs	6·0583	0·355(Γ)	[33]
InSb	6.479 43	0·170(Γ)	[33]
ZnSe	5·6676	2·70	[34]
ZnS	5·4093		
ZnTe	6·1037	2·26	[34]
CdTe	6·4770		
Si	5·4311	1·124(X)	[33]
Ge	5·6579	0·666(L)	[33]

[a]Theoretical estimate.

while the bandgap of AlAs is considerably bigger than that of GaAs. Thus by changing the value of x, the bandgap of the epilayer can be changed over a wide range without affecting the lattice constants. This so called bandgap engineering is the basis of all heterostructure devices [32].

The lattice constants and bandgaps of important semiconductors [33] used in fabricating strained heterostructure devices are given in table 1. The lattice constant of Ge is 4·18% bigger than that of Si and of InAs, 7% bigger than that of GaAs. Because of this lattice mismatch, epilayers of GeSi over Si and of InGaAs over GaAs cannot be grown easily. Frank and Van der Merwe [35] (see also recent review [36]) predicted in 1949 that a coherent (or pseudomorphic) epitaxial layer of a crystal can be grown on a substrate of slightly different lattice constant provided the thickness of the layer is sufficiently small. The layer remains pseudomorphic if its thickness h does not exceed a critical thickness h_c. By choosing suitable values of x, the difference between the lattice constants of the alloys Ge_xSi_{1-x} or $Ga_xIn_{1-x}As$ and the corresponding substrate was reduced and high quality pseudomorphic strained layers of both the alloys were grown in the 1970s [37–39]. With the advent of new growth methods, namely molecular beam epitaxy (MBE), low temperature chemical vapour deposition (CVD) and metallo-organic chemical vapour deposition (MOCVD), the quality of these layers improved rapidly during the 1980s.

GeSi strained layer heterojunction devices can now be fabricated using existing Si technology. This development is important because advances in GeSi strained layer devices can be incorporated in monolithic Si integrated circuits.

There is a snag in the strained layer devices, however. Strain can relax by the introduction of misfit dislocations as suggested by Frank and Van der Merwe, resulting in degradation of the devices. In most cases the dislocations in the layers as grown are not in thermal equilibrium. It is therefore important to understand the mechanism of strain relaxation and determine the stability of the strained layers.

The work reported on the mechanical structure of semiconductor strained layers up to the late 1980s has been reviewed by many authors [4, 5, 36, 40]. In this review

we concentrate on the work done during the past 4 to 6 years particularly on the GeSi system. The definitions and description of strain, dislocations and critical thickness are given in the next subsection. Detailed descriptions of these quantities and the derivation of the critical thickness and density of dislocations is given in sections 2–4. The kinetic processes leading to the relaxation of the strain in metastable layers are discussed in sections 5–7.

Much less detailed work has been performed on metallic layers because the detailed dislocation density is much less important than in the case of the semiconductors. The domain walls here are an intrinsic feature of the stable phase, and research has been largely directed at equilibrium properties. In section 8 we briefly review the few available measurements.

The Frank and Van der Merwe theory has been applied not only to the growth of epitaxial layers, but also to the structure of physisorbed films as described in section 9, and the commensurate–incommensurate phase transitions in both structurally and magnetically modulated materials in section 10. This theory was developed by Bak and Emery [29], and it is instructive to compare the ways in which it has been developed in these different fields: in section 11 we comment on possible developments of the theory for semiconductors.

§ 2. Strain and dislocations

2.1. *Misfit strain*

The epilayer growth of a semiconductor with lattice constant a_l on a thick substrate with lattice constant a_{sub} is illustrated in figure 2 for $a_l > a_{sub}$. The lattice mismatch is measured by the misfit parameter f_m where:

$$f_m = \frac{a_l - a_{sub}}{a_{sub}}. \tag{2}$$

Fig. 2

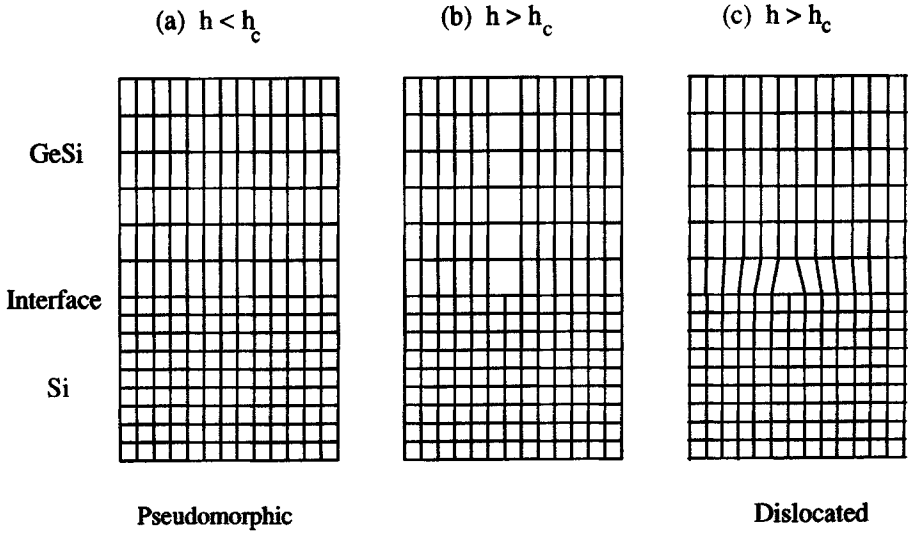

GeSi epilayer grown on a thick Si substrate. (*a*) $h \leqslant h_c$, (*b*) $h > h_c$, removal of a vertical plane from the epilayer and (*c*) $h > h_c$, the strain is accommodated by the introduction of a misfit dislocation.

If both the misfit parameter f_m and thickness h of the epilayer are small, the misfit between the two semiconductors is accommodated by a compressive tetragonal strain of the epilayer as shown in figure 2 (*a*). The strain is homogeneous and is known as the 'misfit strain'.

Consider the growth of Ge_xSi_{1-x} on Si (100) substrate or $In_xGa_{1-x}As$ on GaAs (100) substrate. Vegard's law is valid to a good approximation for both alloys so that the lattice constants $a(x)$ of the alloys are given by

$$a_l(x) = a_{Si(\text{or GaAs})} + (a_{Ge(\text{or InAs})} - a_{Si(\text{or GaAs})})x, \tag{3}$$

showing that the lattice constant of the alloy is larger than that of the substrate in both cases. The misfit parameter f_m is a function of the alloy composition x and, using the values of lattice constants given in table 1, f_m is given by

$$f_m(x) = 0{\cdot}0418x, \tag{4}$$

for Ge_xSi_{1-x}/Si and

$$f_m(x) = 0{\cdot}07x, \tag{5}$$

for $In_xGa_{1-x}As$/GaAs. If the lattice constant of the substrate is larger than that of the epilayer, e.g. epilayers of Ge_xSi_{1-x} alloy grown on a Ge substrate, the tetragonal strain in the epilayer is tensile.

The elastic energy E_H per unit area stored in the epilayer due to homogeneous strain is well known [1, 40],

$$E_H^{ps} = Bhf_m^2, \tag{6}$$

where the elastic constant B is given by†

$$B = 2\mu\frac{1+\nu}{1-\nu}. \tag{7}$$

Here ν is Poisson's ratio, μ is the shear modulus of elasticity and h is the thickness of the layer. The superscript ps in equation (6) indicates that the expression applies to pseudomorphic or perfectly epitaxial layers.

2.2. *Critical layer thickness* h_c

Equation (6) shows that strain energy E_H is proportional to h. As h increases and exceeds a certain *critical thickness* h_c, misfit dislocations begin to set in. A lattice plane of the epilayer is removed as shown in figure 2 (*b*). (This is the Volterra construction. Of course, in real life, no planes are 'removed'; instead, slip occurs.) The lattice relaxes with the introduction of a misfit dislocation as shown in figure 2 (*c*). For $h > h_c$, this configuration becomes energetically favourable. Misfit strain is now partly accommodated by the dislocations.

Two theories have been developed to calculate the equilibrium critical thickness h_c. The first theory originated in the work of Frank and Van der Merwe [35] and has been developed further by Van der Merwe and collaborators [36]. It is based on the principle of energy minimization. The second is due to Matthews and Blakeslee [41, 42] and is known as the force balance theory. Initially the two theories gave different numerical values of the critical thickness for the same epilayer (see [10] and references given in [40, 43]). We will see in section 3 that if correctly formulated,

† Note that B is not the bulk modulus: it allows for the vertical relaxation of the layer which accompanies the constraint in the plane, and incorporates the factor of $\frac{1}{2}$ in relating elastic energy to the square of strain.

the two theories are equivalent and always give identical numerical values of the critical thickness, as by definition of thermodynamic equilibrium they must.

2.3. *Misfit dislocations*

If the thickness of the epilayer is continuously increased, the energy minimization predicts that the number of misfit dislocations and the strain relaxation will also increase. The strain is never fully relaxed for any finite value of the thickness but approaches f_m (which corresponds to complete relaxation of strain) as h approaches ∞. To calculate the number of dislocations as a function of h, we must write an expression for the total energy of the epilayer and minimize the energy with respect to strain.

Consider an epilayer with two equivalent orthogonal periodic arrays of misfit dislocations. Let the spacing between two neighbouring dislocations in the arrays be p. Each dislocation relaxes the strain by b_1/p where

$$b_1 = -b \sin\alpha \sin\beta, \tag{8}$$

b is the magnitude of the Burgers vector, α is the angle between the glide plane and the normal to the interface and β is the angle between the dislocation line and the Burgers vector. Numerical values of the angles are,

$$\alpha = \arctan\frac{1}{\sqrt{2}}, \quad \beta = \frac{\pi}{3}. \tag{9}$$

for 60° dislocations [44]. For 90° dislocations [45],

$$\alpha = \frac{\pi}{2}, \quad \beta = \frac{\pi}{2}. \tag{10}$$

The average strain relaxation is b_1/p. In the presence of dislocations the homogeneous strain in the epilayer becomes

$$\varepsilon = f_m + b_1/p. \tag{11}$$

The energy due to homogeneous strain ε is then given by

$$E_H^{pr} = Bh\varepsilon^2 = Bh(f_m + b_1/p)^2, \tag{12}$$

where superscript pr indicates that dislocations are present and strain is partially relaxed. It should be noted that f_m and b_1/p always have opposite signs and the homogeneous energy is always reduced by the misfit dislocations. The cross term in $(f_m + b_1/p)^2$ gives the energy of interaction between the two strains.

2.4. *The energy of the dislocations*

2.4.1. *Dislocations in epilayers with free surfaces*

The expression for the energy (per unit length) of an isolated dislocation as derived for example by Willis *et al.* [46] is,

$$E_D^{\infty} = A\left[a_0 + a_1 \ln\frac{\rho_c h}{q} - a_3\right]. \tag{13}$$

This derivation uses linear elasticity theory to calculate the energy and breaks down at the core of the dislocation line. The radius of the core is assumed to be q, usually taken to equal $b/2$, and the non-elastic energy in the core is taken into account by introducing the dimensionless parameter ρ_c. The core parameter ρ_c becomes impor-

tant only when the distance from the dislocation line is small and is taken to be unity in the fomulation of Willis *et al.* [46]. The constants used in equation (13) are defined in terms of the elastic constants and the properties of the dislocation as

$$A = \frac{\mu}{4\pi(1-\nu)} \tag{14}$$

$$b_1 = -b\sin\alpha\sin\beta, \quad b_2 = b\cos\alpha\sin\beta, \quad b_3 = -b\cos\beta. \tag{15}$$

$$\left.\begin{aligned} a_0 &= (b_1^2 + b_2^2)\left(\sin^2\alpha - \frac{1-2\nu}{4(1-\nu)}\right), \\ a_1 &= (b_1^2 + b_2^2) + (1-\nu)b_3^2, \\ a_3 &= \tfrac{1}{2}(b_1^2 + b_2^2). \end{aligned}\right\} \tag{16}$$

The Burgers vector b is 3·84 Å for silicon. The equation for the dislocation energy used by Matthews [41, 42], and by Ball and Van der Merwe [36] can be written as

$$E_D^{\infty} = Ab^2\left[(1-\nu\cos^2\beta)\ln\frac{\rho_c h}{q}\right]. \tag{17}$$

Apart from the small differences in the additive constants, it can be shown that equations (13) and (17) are identical.

The energy $E_D(p)$ (per unit area) of a layer containing two orthogonal arrays of periodic dislocations is given by [44, 46],

$$E_D(p) = Bh\frac{b_1^2}{p^2} + \frac{2}{p}E_{DS}, \tag{18}$$

where $E_{DS} = E_{DS}^{\infty}$ if the interactions between the dislocations are neglected. In practice, however, the interactions between the dislocations are important [46–48] and E_{DS}^{∞} must be replaced by [44, 46]†

$$E_{DS} = A\left[a_0 + a_1\ln\left(p\frac{1-\exp(-s)}{2\pi q}\right) + a_2\frac{s\exp(-s)}{1-\exp(-s)} - a_3\frac{s^2\exp(-s)}{(1-\exp(-s))^2} - a_2\right], \tag{19}$$

where

$$a_2 = b_1^2 - b_2^2, \quad s = 4\pi\frac{h}{p} \tag{20}$$

and E_{DS} is the energy, per unit length, due to the fluctuating elastic field. For any given value of p the energy $E_D(p)$ given by equation (18) is considerably larger than the energy $(2/p)E_D^{\infty}$ obtained by adding together the energy of all the dislocations. The latter procedure, which has been used previously [4, 36, 43], is not correct and can cause large errors in the calculation of the strain relaxation.

2.4.2. *Capped layers*

Almost all strained layer devices use thick unstrained layers on top of the strained layers. Such strained layers are known as capped or buried strained layers. During the growth the layers have a free surface but thick metastable layers can be grown without dislocations. The layers are then capped for fabricating the device

† There was an error in the original derivation of equation (19) in [46]. The error was corrected in [44].

Fig. 3

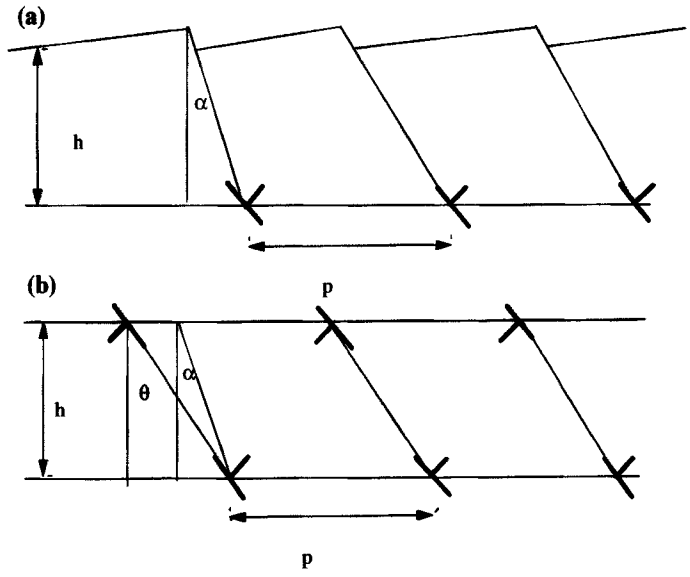

Schematic representation of (*a*) 60° dislocations in an uncapped layer and (*b*) 60° dipoles in a capped layer [49].

and, by modifying the energy of the dislocations as well as the magnitude and kinetics of strain, relaxation can stabilize the dislocation-free structures.

If the cap is sufficiently thick, relaxation of strain occurs by the introduction of dislocation dipoles. A dipole consists of a pair of dislocations, one each at the upper and lower interfaces [49, 50]. A schematic representation of a 60° array of dislocations in an uncapped layer and dipoles in a capped layer is given in figure 3. Both dislocations of the dipole are of the 60° type and α is the same as for the uncapped layers. The dislocations at the lower interface have a Burgers vector **b** and those at the upper interface have a Burgers vector $-\mathbf{b}$. In this case the dislocation spacing p is the same in both the upper and the lower array of dislocations (see figure 3). The angle θ is the angle between the line joining the two dislocations of a dipole and the perpendicular to the interface. For $\alpha = \theta$, the energy due to the fluctuating part of the strain is given by [50],

$$E_{\mathrm{DS}}^{\mathrm{cap}} = 2A\left[2a_4 + a_1 \ln\left(p\frac{1-\exp(-w)}{2\pi q}\right) - 2a_3 w \,\mathrm{Re}\left(\frac{\exp(-2i\alpha)\exp(-w)}{1-\exp(-w)} + a_5\right)\right], \tag{21}$$

where

$$w = 2\pi\frac{h}{p},$$

$$a_4 = -\tfrac{1}{2}(b_1^2 + b_2^2)\frac{1-2\nu}{4(1-\nu)},$$

and

$$a_5 = (b_1^2 + b_2^2)\cos^2\alpha. \tag{22}$$

The total energy $E_D^{cap}(p)$ of the arrays in a capped layer is obtained if E_{DS} in equation (18) is replaced by E_{DS}^{cap}, to give

$$E_D^{cap}(p) = Bh\frac{b_1^2}{p^2} + \frac{2}{p}E_{DS}^{cap}. \tag{23}$$

The above expression assumes that the thickness of the cap is infinite. Recently the energy of a single dipole as well as of arrays of periodic dipoles in a layer with arbitrary thickness of the cap have also been calculated [51]. These calculations show that the energy of an array of dipoles in a layer with a thick cap is considerably larger than the energy of the array of single dislocations in an equivalent layer with free surface for the same dislocation spacing.

2.4.3. *Energy of non-periodic arrays of dislocations*

Before the work of Atkinson and Jain [52–54] and Jain *et al.* [45, 55], all calculations of the energies and strain of the dislocation arrays were made for periodic distributions of dislocations. The periodic distribution has the lowest energy and is the stable state if the layers are in thermodynamic equilibrium. In real systems the distribution of dislocations in relaxed epilayers is rarely periodic and a typical distribution of misfit dislocations in a 0·75 μm thick $Ge_{0.15}Si_{0.85}$ layer is shown in figure 4. The dislocations nucleate at regenerative heterogeneous sources (defects, impurities, ledges, etc.), and hence form in bunches and presumably these bunches are distributed in a random manner in the layer. It is therefore important to discuss epilayers containing non-periodic dislocation arrays.

Fig. 4

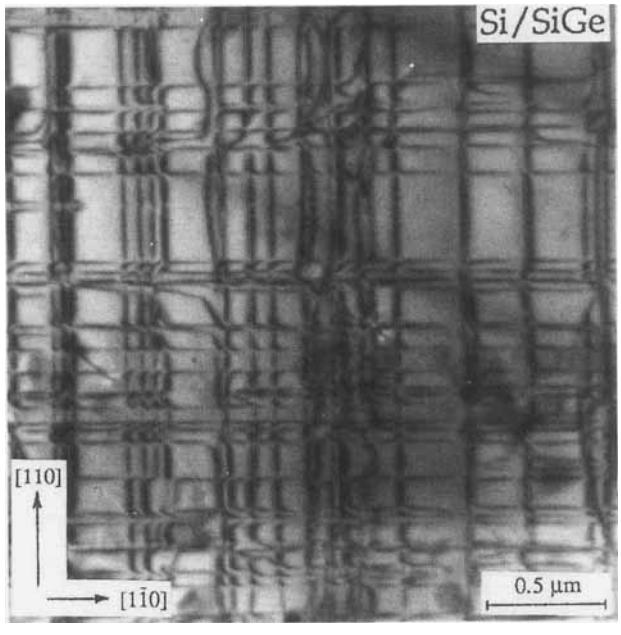

Misfit dislocation distribution in a relaxed 0·75 μm thick $Ge_{0.15}Si_{0.85}$ layer. This figure has been provided kindly by Dr G. R. Booker of Oxford University.

The energy of interaction $E_I(h,p)$ (per unit length of the dislocation lines) of a pair of dislocations is given by [52–55],

$$E_I(h,p) = Ab_1^2\left[\ln\left(4(h/p)^2+1\right)+\frac{4(h/p)^2(4(h/p)^2+3)}{(4(h/p)^2+1)^2}\right] + Ab_2^2\left[\ln\left(4(h/p)^2+1\right)-\frac{4(h/p)^2(12(h/p)^2+1)}{(4(h/p)^2+1)^2}\right] + Ab_3^2[\ln\left(4(h/p)^2+1\right)(1-\nu)]. \tag{24}$$

If we now consider an irregular (or non-periodic) array of $N+1$ dislocations with p_i as the inter-dislocation spacing between the ith and $(i+1)$th dislocations, the total interaction energy of the array is given by [55],

$$E_I^{irr}(N,h,\{p\}) = \frac{2}{N\bar{p}}\left[\sum_{i=1}^{N}E_I(h,p_i)+\sum_{i=1}^{N-1}E_I(h,p_i+p_{i+1}) + \sum_{i=1}^{N-2}E_I(h,p_i+p_{i+1}+p_{i+2})+\sum_{i=1}^{N-3}E_I(h,p_i+p_{i+1}+p_{i+2}+p_{i+3}) + \cdots+\sum_{i=1}^{N-(N-1)}E_I(h,p_i+p_{i+1}\cdots+p_{i+(N-1)})\right]. \tag{25}$$

The energy of the two perpendicular arrays per unit area of the layer is obtained by adding to the interaction energy given above, the self-energy $(2/\bar{p})E_D^{\infty}$ ($\bar{p}$ is the average inter-dislocation distance in the array) of the dislocations and the energy of interaction $E_{I\perp}(\bar{p})$ between one array and the other perpendicular array. The energy of interaction $E_{I\perp}(\bar{p})$ is given by [52–55],

$$E_{I\perp}(\bar{p}) = \frac{2\mu h}{\bar{p}}\left[\frac{\nu b_1^2}{1-\nu}-\frac{b_3^2}{2}\right], \tag{26}$$

which is dependent only on the average spacing $\bar{p}$ and not the details of the distribution of spacings, p_i. Numerical values of the energy of two orthogonal arrays of periodic and non-periodic interacting dislocations are shown in figure 5. Rockett and Kiely [56] have calculated the interaction energy using an approximate theory. They approximated the observed non-periodic array with a periodic array and took into account directly only the interactions between first neighbours. Curves 1 to 3 show that interactions between distant neighbours are important. For modelling purposes, non-periodic arrays with average spacing $\bar{p}$ are often replaced by periodic arrays with spacing $p=\bar{p}$. Comparison of curve 3 with curve 4 shows that approximating a non-periodic array by a periodic array can lead to considerable errors [45].

2.4.4. *Total energy of the strained layers containing dislocations*

The total energy of the layer is made up from the following contributions:

(1) Energy due to misfit strain.
(2) Energy due to the average (homogeneous) strain produced by the dislocation arrays.

Fig. 5

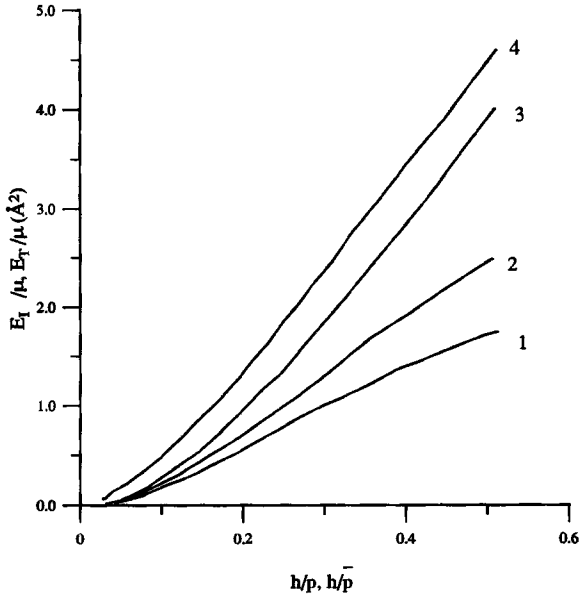

Interaction energy of two orthogonal periodic and non-periodic arrays of 90° dislocations. Curves 1, 2 and 3 are for periodic arrays with p as inter-dislocation spacing. Curve 1 includes interactions between nearest neighbours only, curve 2 includes interactions between nearest and next nearest neighbours and curve 3 includes all interactions. Curve 4 is for 41 non-periodic dislocations. A Gaussian distribution of non-periodic dislocations with spacing $\bar{p} = p$ and standard deviation $\sigma = 0{\cdot}44p$ is assumed for the non-periodic distribution [45].

(3) Energy of the interactions between the misfit and the homogeneous strains produced by the dislocations.
(4) Energy E_{DS} or E_{DS}^{cap} due to fluctuating part of the strain of dislocation arrays. The average strain has been accounted for in item 2 above, and so the fluctuating part of the strain has an average zero and therefore does not interact with the homogeneous strains.

Using equations (12), (19), and (21) we obtain the following expressions for the total energy (per unit area) of an uncapped layer,

$$E_T = Bh\left(f_m + \frac{b_1}{p}\right)^2 + \frac{2}{p}E_{DS}, \tag{27}$$

while for a capped layer we obtain

$$E_T^{cap} = Bh\left(f_m + \frac{b_1}{p}\right)^2 + \frac{2}{p}E_{DS}^{cap}. \tag{28}$$

The total energy of the layer containing arrays of non-periodic dislocations can be calculated in a similar manner. The term $Bh(f_m + (b_1/p))^2$ corresponding to the first three contributions remains the same in all cases. The last term is obtained by

Fig. 6

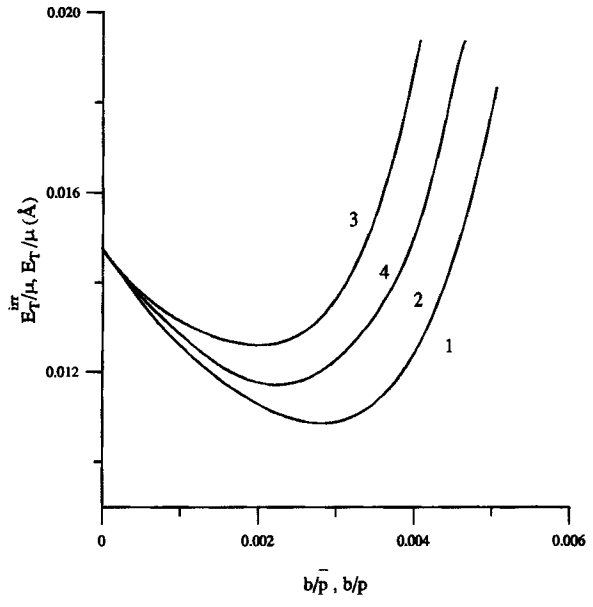

Plot of normalized total energy E_T^{irr}/μ versus $h/\bar{p}$ (non-periodic distribution) and E_T/μ versus h/p (periodic distribution). Curve 1 is for a periodic array, curve 2 is for a Gaussian distribution, and curve 4 is for a uniform-random distribution, both with the same standard deviation $\sigma = 0{\cdot}44\bar{p}$. Curve 3 is for a Gaussian distribution with $\sigma = 0{\cdot}7\bar{p}$. Thickness $h = 254$ Å and $f_m = 0{\cdot}0042$ [55].

subtracting $Bh(b_1/p)^2$ from the energy of the non-periodic arrays given in section 2.4.3.

The expression for the total energy of an uncapped layer used in the original Van der Merwe's theory is [4, 35, 42],

$$E_T^m = Bh\left(f_m + \frac{b_1}{p}\right)^2 + \frac{2}{p}E_D^\infty. \tag{29}$$

The correct equation (27) is quite different from equation (29) used in the earlier literature: specifically, the difference is between E_D^∞, given by equation (17), and E_{DS}, defined in equation (19).

The total energy of an epilayer containing non-periodic arrays can be calculated by adding the homogeneous misfit strain energy and the interaction energy between the homogeneous misfit strain and the average strain caused by the dislocation arrays. The energy calculated in this manner for an epilayer with $f_m = 0{\cdot}0042$ is shown in figure 6. Curve 1 is for periodic arrays. Two different non-periodic distributions were considered in the calculations. Curves 2 and 3 are for Gaussian distributions and curve 4 is for a uniform-random distribution. It is seen from this figure that in equilibrium the number of misfit dislocations present in the layer is smaller if the distribution is non-periodic. The number decreases as the standard deviation σ increases but it is not very sensitive to the details of actual distribution.

§ 3. Critical thickness

3.1. *Theories of the critical thickness* h_c

In this section we discuss the force balance theory of Matthews and Blakeslee [41, 42, references to their earlier papers are given in these papers] and the theory of Ball and Van der Merwe [36] based on the principle of energy minimization. We show that the two theories are equivalent. Misfit dislocations are formed either by nucleation of surface half loops and their expansion as shown in figures 7 (*a*) and (*b*) or by propagation of existing threading dislocations as shown in figure 7 (*c*). In their force balance theory, Matthews and Blakeslee [41, 42] considered a substrate–epilayer structure in which threading dislocations crossing the interface are present and move to produce the misfit dislocations. The threading dislocation experiences two competing forces. When the threading dislocation propagates through the layer, a segment of misfit dislocation is created reducing the strain and the energy of the epilayer. This provides the driving force for the motion. The force is equal to $Bhf_m b_1$. The line tension E_D^∞ (which is equal to the energy per unit length) of the misfit dislocation opposes the motion. The net force G acting on the threading dislocation is,

$$G = Bh|f_m b_1| - E_D^\infty. \tag{30}$$

Fig. 7

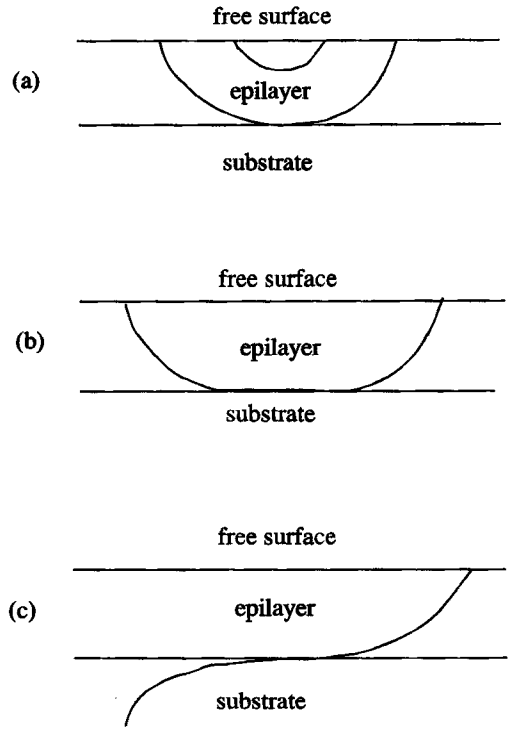

(*a*) A half loop nucleated at the surface expands and touches the interface, (*b*) its threading arms move further apart and deposit a misfit dislocation at the interface and (*c*) an existing threading dislocation moves to produce a misfit dislocation.

Below the critical thickness, G is negative and the layer remains pseudomorphic. As h increases, the driving force given by the first term in equation (30) increases faster than the opposing force given by the second term. Matthews and Blakeslee assumed that at $h = h_c, G = 0$. For $h > h_c, G$ is positive and the threading dislocation moves, depositing the misfit dislocation. Equating G to 0, we obtain the Matthews and Blakeslee equation for the critical thickness,

$$h_c = \frac{1}{8\pi(1+\nu)b_1 f_m}\left(a_0 + a_1 \ln \frac{2\rho_c h_c}{q} - a_3\right), \tag{31}$$

which can be written using the form for the dislocation energy used by Ball and Van der Merwe [36] and Matthews [41, 42] as

$$h_c = \frac{b^2(1-\nu\cos^2\beta)}{8\pi(1+\nu)b_1 f_m} \ln \frac{\rho_c h_c}{q}. \tag{32}$$

The principle of energy minimization states that below the critical thickness, the energy of the epilayer should increase by the introduction of the misfit dislocation and beyond the critical thickness, the energy should decrease. At the critical thickness, the total energy of the layer is a minimum and the change in energy on introducing a dislocation is 0. It can easily be seen that G also represents the change in energy of the epilayer that occurs by the introduction of unit length of the misfit dislocation and should be 0 according to the principle of energy minimization. In practice, we write an expression for the total energy of a sample of linear dimension L (L is large so that end effects are negligible) and equate its derivative (with respect to $1/L$) to 0 to obtain the minimum in energy. We again obtain exactly the same equations, namely, $G = 0$ for determining the critical thickness.

Although equation (29) does not include the effect of the interactions between the dislocations, these interactions become negligible as $p \to \infty$, and so the same expression for h_c is obtained by equating to zero the first derivative of equation (27) with respect to $1/p$ as $p \to \infty$. This procedure does not however always give the correct result as the interactions between the dislocations are attractive and the transition from the dislocation free state to one including dislocations can be first order. If we expand equation (27) in powers of $1/p$ then

$$E_T = Bhf_m^2 + (2Bhf_m b_1 + 2E_{DS}^{\infty})\frac{1}{p} + (Bhb_1^2 + 2E_1')\frac{1}{p^2} + 2E_1''\frac{1}{p^3} + \cdots, \tag{33}$$

where E_1' and E_1'' are the coefficients of the expansion of the interaction energy in powers of $1/p$. If $Bhb_1^2 + 2E_1'$ is positive, the transition is continuous and the equilibrium value of $1/p_s$ is given by

$$\frac{1}{p_s} = \frac{2Bf_m b_1(h - h_c)}{Bh^2 b_1^2 + 2E_1'} \tag{34}$$

for small $1/p$, and so increases linearly with $h - h_c$. In contrast if the quadratic term in equation (33) is negative, $E_1' < -\frac{1}{2}Bhb_1^2$, the transition is first order and occurs for a thickness less than h_c.

Detailed numerical calculations [44] show that both types of behaviour can occur. In figure 8 we plot the energy of a layer of $Ge_{0.1}Si_{0.9}$ for the thickness $h = h_c = 236$ Å as given by equation (32) as the number of 60° dislocations is increased. The solid curve shows the energy including the effect of the interactions

Fig. 8

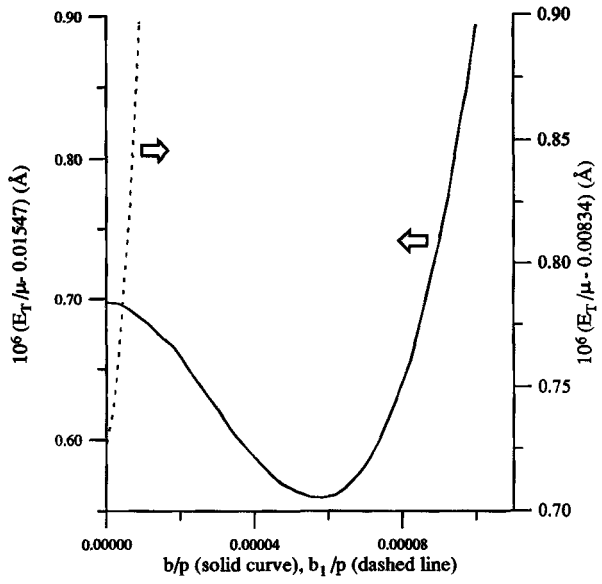

E_T/μ versus $|b_1/p|$ for Ge_xSi_{1-x} strained layers for $h = 236$ Å and $x = 0{\cdot}1$, neglecting interactions (dashed curve) and including interactions (solid curve) [45].

between the dislocations and the dashed curve neglects the interactions. The dashed curve increases monotonically with $1/p$ as the equilibrium state has $\langle 1/p \rangle = 0$. In contrast, the solid curve has a maximum at $1/p = 0$ and a shallow minimum at $b_1/p = 0{\cdot}000\,056$. There is therefore a first order transition for h slightly less than 235 Å to a state with $p_s = 19\,200$ Å.

Similar calculations for periodic arrays of 90° dislocations give a continuous transition when h_c is given by equation (31). We conclude that in practice h_c is nearly always given reasonably accurately by equation (31), but that the transition as a function of h may be either continuous with $1/p \propto h - h_c$ or discontinuous with a non-zero value of $1/p$ at $h = h_c$.

3.2. *Experimental values of* h_c

Curves 1 and 2 in figure 9 show the values of h_c for 90° and 60° dislocations† calculated using equation (31). Values of h_c of Ge_xSi_{1-x} strained layers were determined experimentally by Bean *et al.* in 1984 and by other authors (see the reviews [40, 9]). In the work of Bean *et al.* [9, 40] layers were grown at 550°C and 60° dislocations were observed (60° dislocations are always observed at low mismatch). Curve 3 in figure 9 represents the empirical fit of their data. Observed thicknesses are much larger than the calculated values particularly at low values of misfit parameter. Numerous determinations of h_c of uncapped $In_xGa_{1-x}As$ layers grown on GaAs (100) were made in 1986 and 1987. Similar discrepancies were observed in many

† This figure explains why calculated values of h_c obtained earlier using the two equilibrium theories were different. A survey of the literature shows that in most cases h_c for 90° was calculated while using Van der Merwe's theory and for 60° dislocations, while using the theory of Matthews and Blakeslee.

Fig. 9

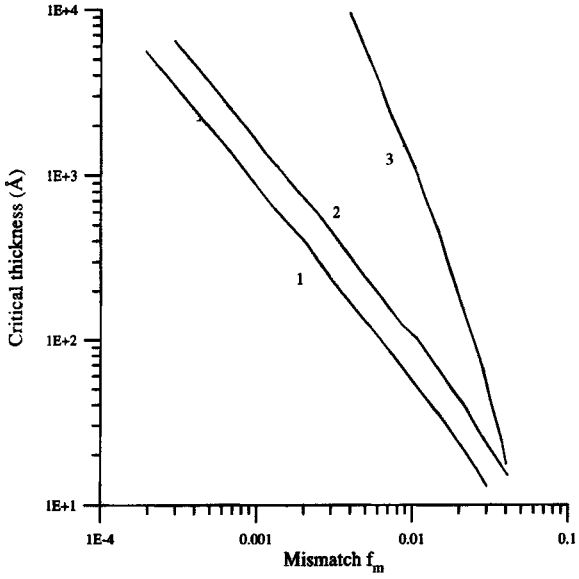

Calculated values of h_c as a function of f_m for 90° (curve 1) and for 60° (curve 2) for both Ge_xSi_{1-x} and $In_xGa_{1-x}As$ layers. Curve 3 represents empirical fit to the experimental data of Bean [9] for Ge_xSi_{1-x} layers. The figure is taken from [45].

cases, the critical thickness being larger than that calculated using equation (31). Fritz [57, 58] has reviewed this data and has shown that the discrepancy arose mostly in those cases where X-ray diffraction techniques were used to measure the onset of strain relaxation. The sensitivity of this technique in the measurements was not better than about 10^{-3}, and so the strain could not be detected if h was only slightly larger than h_c. Newer X-ray techniques, particularly using synchrotron sources, have much better resolution of order 10^{-4}, but have not been extensively used to measure h_c. Another problem arises from the difficulty of nucleating dislocations at relatively small $h - h_c$ and low growth temperatures [57, 58]. More reliable measurements of h_c were made by Houghton *et al.* [59] using X-ray topography and Nomarski miscroscopy of defect etched surfaces to monitor the onset of misfit dislocations in Ge_xSi_{1-x} strained layers. These techniques are so sensitive that one dislocation in an area of 1 cm^2 can be detected. They found very good agreement between theory (curve 2 in figure 9) and experiment. In the case of $In_xGa_{1-x}As$ also, experimental values obtained using sensitive techniques such as photoluminescence spectroscopy and Hall measurements agree closely with the theoretical values [57, 58].

The critical thickness of the capped layers can be calculated using equation (31) provided we use equation (28) (with $p = \infty$) instead of (27) for the total energy. Extensive measurements of the critical thickness of capped Ge_xSi_{1-x} and $In_xGa_{1-x}As$ have also been made. The calculated values of critical layer thickness for both uncapped and capped Ge_xSi_{1-x} layers are shown in figure 10. The critical thickness of a capped layer is approximately twice that of the corresponding uncapped layer for low mismatch and is four times as large for large mismatch when the Ge fraction x is greater than 0·8. Experimental results of Houghton *et al.* [60] for the capped layers are also included in the figure. For a given misfit the critical

Fig. 10

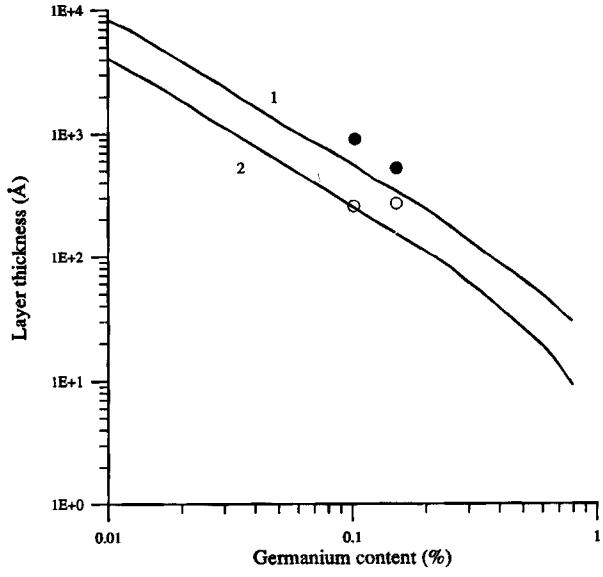

Critical thickness h_c (60° dislocations) of a capped layer (curve 1) and an uncapped layer (curve 2) plotted as a function of Ge fraction x. Experimental data [60] for the capped layer are shown by open and filled circles [49].

layer thickness lies between the greatest thickness for which a layer was found to be dislocation-free (open circles) and the smallest thickness for which partial relaxation of strain by the introduction of the dislocations was detected (full circles). The open and full circles provide upper and lower bounds for the critical thickness. The theoretical curve falls within the bounds placed by experiment.

Experimental data for $In_xGa_{1-x}As$ quantum wells (capped layers) obtained using sensitive techniques [61] are shown in figure 11. The solid curve shows the predicted values using an equation derived by Matthews and Blakeslee [62] (see equation (5) on p. 124). This equation was derived approximately for a specific superlattice in which strain in the $In_xGa_{1-x}As$ was half of the misfit parameter. The equation therefore overestimates h_c. If correct values of h_c for the capped layer shown in figure 10 are used,† agreement between theory and experimental values becomes better.

The critical thickness of graded strained layers (layers in which Ge concentration varies with the distance z from the interface) has been studied in [36, 63]. It can be shown that for any grading, equation (31) can also be used for the graded layers provided we use the average of Ge concentration for determining the misfit parameter.

§ 4. Thick epilayers in equilibrium

In figure 12, the total energy E_T/μ of the $Ge_{0.1}Si_{0.9}$ epilayers calculated for 60° interacting dislocations using equation (27) is plotted as a function of strain relaxation $|b_1/p|$ for 7 different values of the epilayer thickness h [44]. The calculated

† Theoretical curves in this figure can be made applicable to $In_xGa_{1-x}As$ layers by changing abscissa from x to f_m.

Fig. 11

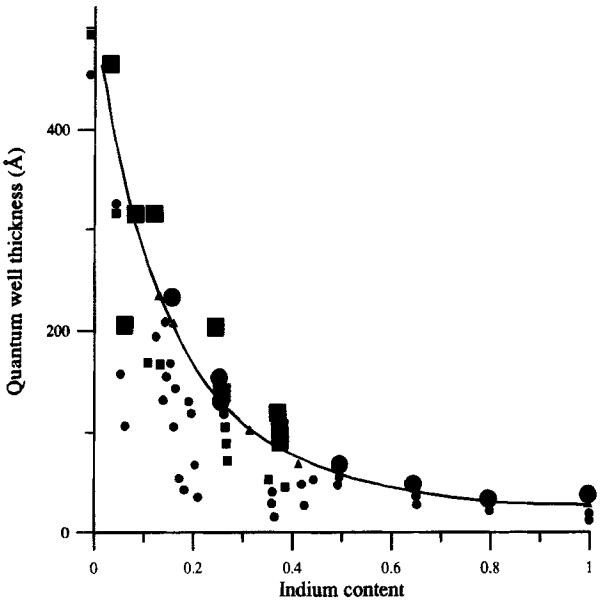

Thickness versus In content in $In_xGa_{1-x}As$ strained layers. Small circles and squares represent high quality layers with no strain relaxing defects. Triangles represent quantum wells with small number of defects and large symbols represent quantum wells with large concentration of defects. Calculated values are shown by the continuous curve (see text) [61].

Fig. 12

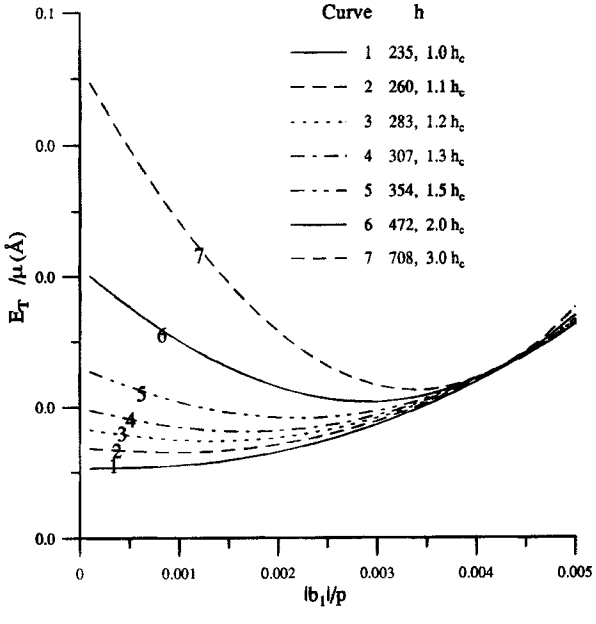

Total energy E_T/μ of the $Ge_{0.1}Si_{0.9}$ epilayers is plotted as a function of strain relaxation $|b_1|/p$ for 7 different values of h [44].

value of h_c is 236 Å for this composition. The value of f_m is indicated by an arrow in the figure. Each curve shows a minimum, the minimum becoming stronger and moving to larger values of $|b_1/p|$ as h increases. The position of the minimum tends to move to f_m as h approaches ∞. These results show that for each thickness, there is a definite concentration $1/p_s$ of dislocations needed for the epilayer to be stable (the corresponding strain relaxation is $|b_1/p_s|$). These minima in energy give pairs of values of h_e and $|b_1/p_s|$ for stable configurations.

If the theory is applied to very thin films then the thickness h can become comparable with the core radius ρ, and the theory is inadequate as can be seen by allowing $h \to 0$ in equation (13). Payne *et al.* [64] have pointed out that this inadequacy of the theory can be important if the misfit strain is sufficiently large and have used the modification proposed by Peierls and Nabassor to describe the dislocation more satisfactorily.

The values of $|b_1/p_s|$ at which minima occur for different values of h increase with h first rapidly and then slowly. For any given thickness, the concentration $|b_1/p_s|$ of dislocations is smaller if interactions of dislocations are not properly taken into account and E_D^∞ instead of E_{DS} defined in equation (19) is used in the energy expressions. However the concentration decreases for a non-periodic distribution. The observed concentrations are always much smaller than the predicted value for a periodic distribution. The discrepancy is due partly to the non-periodic distribution and partly to the difficulty in nucleating the dislocations.

The equilibrium strain relaxation $\gamma_e = b_1/p_s$ in a capped layer can be found by locating the minima in the plots of total energy E_T^{cap} against $|b_1/p|$ given by equation (28). For equal thickness and misfit strain, the number of dislocations introduced in the capped layers is always much smaller [49].

§ 5. Motion of dislocations

5.1. *The glide velocity*

In thick ($h > h_c$) semiconductor epilayers grown at 550°C or lower temperatures, the concentration of misfit dislocations is much smaller than that predicted by the thermodynamic equilibrium condition. The energy needed for nucleation or multiplication of dislocations is not available at these temperatures. Therefore the layers are metastable. When the metastable layers are heated at higher temperatures or during the ageing of the layers, dislocations are introduced and the strain relaxes. Generation of dislocations involves nucleation and/or multiplication and glide motion of dislocations. Figure 7 in section 3 shows how misfit dislocations are deposited by the propagation of threading dislocations. The creation of misfit dislocations by multiplication also involves glide motion of dislocations and the nature of the dislocations depends on the growth mechanism of the layer. If the growth mechanism is two-dimensional it is difficult to nucleate misfit dislocations and the growth is often detectable. This growth mode occurs at low temperatures. At high temperatures, the growth mode is by three-dimensional island growth because the atoms can more easily migrate to the islands [65]. Misfit dislocations are then readily nucleated at the boundaries between the islands [96].

In the next few sections we discuss the processes involved in establishing an equilibrium distribution of dislocations. In this section we discuss the motion of dislocations [67–69]; nucleation, multiplication and blocking [70–72] are discussed in the next section, and annealing and strain relaxation [44, 72, 73] in section 7.

The misfit dislocation velocity v_d given by the equation [73],

$$v_d = v_0(\sigma_{exc})^m \exp(-E_v/kT), \tag{35}$$

where v_0 is a constant, σ_{exc} is the excess stress and E_v is the energy of activation for the glide motion of the dislocation. Values of m have been taken as 1 [68, 69] and 2 [67, 74, 75] in equation (35). The excess stress can be written as

$$\sigma_{exc} = 2S\mu\epsilon\frac{1+\nu}{1-\nu} - \frac{\mu b\cos\alpha(1-\nu\cos^2\beta)}{4\pi h(1-\nu)}\ln\frac{\rho_c h}{b}. \tag{36}$$

Here S is the Schmid factor and has a value of $1/\sqrt{6}$. The first term in equation (36) is the stress acting on the dislocation line due to misfit strain and the second term is the self-stress of the dislocation line [76] obtained by differentiating the dislocation array energy $(2/p)E_D^{\infty}$ given by equation (13). The symbols have been defined in equation (14).

If the strained layer has an 'infinitely thick' capping layer, the self-energy of the dislocation line (dipole) increases by a factor of about 2 [49] and therefore σ_t is replaced by $2\sigma_t$ in equation (36). If the thickness of the capping layer is finite, the energy of the dislocation and σ_{exc} can still be calculated but simple closed form solutions cannot be obtained [51]. The stress σ_{exc} and the velocity of the dislocation are always smaller in capped layers.

The effect of the interactions between the dislocations on σ_{exc} is very large. For a periodic distribution of dislocations, the second term is equation (36) is now obtained by differentiating $(2/p)E_{DS}$ given by equation (19) and is much smaller [5]. The velocity therefore increases when interactions between the dislocations are included in the theory [44]. However, a periodic distribution is rarely observed. For a non-periodic distribution, the second term in equation (36) increases and the velocity is reduced (see section 2.4.3). Also, because of local variations in stress, the velocity must be a function of the spatial coordinates of the dislocation. The velocities of dislocations in different regions of a sample have been observed to be different by a factor up to 3 [69].

5.1.1. *The double kink model*

Suppose a dislocation line moves from A to B as shown in figure 13. If the whole line were to move in one step, simultaneous rearrangement of a very large number of

Fig. 13

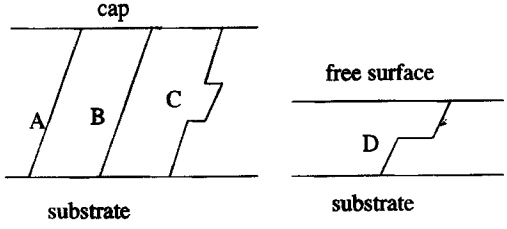

Motion of a dislocation line from A to B involves jumps of a large number of atoms. It is easier for the dislocation to move by nucleation of a double kink C and then by the motion of the two component kinks along the dislocation line, moving a larger and large portion of the line to the right. If the epilayer has a free surface and its thickness is small, a nucleation and motion of a single kink, shown at D, become the preferred processes.

atoms would be involved and the energy of activation would be very high. The double kink model provides a mechanism to avoid this difficulty [5, 69, 77]. According to this model, in the beginning a small portion of the line jumps forward (say to the right) forming a double kink as shown at C in figure 13. Subsequently the two component kinks move apart along the dislocation line. This causes a larger and larger portion of the dislocation line to move forward to the right; and ultimately the whole dislocation moves by one atomic spacing. The process is then repeated. If the dislocation line is sufficiently long, several double kinks may be formed at the same time.

Let $2F'_k$ be the energy required to nucleate an isolated double kink.† The average distance X_k between the double kinks is given by [69],

$$X_k = 2c \exp\left(\frac{F'_k}{k_B T}\right), \tag{37}$$

where c is the kink jump distance (3·8 Å). The rate of nucleation J_k of the kinks is given by [69],

$$J_k = \frac{\nu_D b d_p \sigma_{exc}}{kT} \exp\left(-\frac{E_m + 2F'_k}{K_B T}\right), \tag{38}$$

where d_p is the distance between the Peierls valleys and has a value of 3·3 Å for Ge/Si, ν_D is the Debye frequency and E_m is the energy of activation for kink jumps along the line direction. The transverse dislocation velocity v_d is given by [69],

$$v_d = \frac{2\nu_D c b d_p^2 \sigma_{exc}}{k_B T} \exp\left(-\frac{E_m + F'_k}{k_B T}\right) \frac{L_d}{L_d + X_k}. \tag{39}$$

Here L_d is the length of the dislocation line. If $L_d \gg X_k$, equation (39) shows that the velocity becomes independent of the length of the dislocation line. On the other hand if $L_d \ll X_k$, equation (39) becomes

$$v_d = \frac{\nu_D b d_p^2 \sigma_{exc} L_d}{k_B T} \exp\left(-\frac{E_m + 2F'_k}{k_B T}\right) \tag{40}$$

and the velocity is proportional to the length of the dislocation line. This behaviour has been confirmed experimentally in bulk Ge and Si [78, 79 and references therein]. The observed dislocation mobility increases with its length L_d up to a certain length L_0 and becomes independent of L_0 for $L_d > L_0$. Measured values of L_0 were 0·2 to 0·4 μm in Si and 1·5 μm in Ge. Louchet and co-workers [78, 79] have refined the double kink model. They performed a statistical analysis of the double kink formation and derived a somewhat different expression for the velocity.

For Ge_xSi_{1-x} strained layers and for $L_d > L_0$, the observed velocity v_∞ can be represented by [68]

$$v_\infty = B_0 \sigma_{exc} \exp\left(\frac{-(2{\cdot}156 - 0{\cdot}7x)}{k_B T}\right). \tag{41}$$

Here $B_0 = 1{\cdot}15 \times 10^{-3}\ s\,m^2\,kg^{-1}$ and $k_B T$ is in electronvolts. Experimental results [69] are in reasonable agreement with the above expression.

† The prime on F indicates that it is modified by kink–kink interactions and by the work done by the applied stress if the stress is very high [5, 69].

5.1.2. *The single kink model*

If the layer is not capped and is very thin, the formation of a single kink as shown at D in figure 13 is preferred. Now the single kink runs along the dislocation line, again moving a larger and larger portion of the dislocation line to the new position. Single kinks can be formed only up to a certain depth s_0^* below the surface. The distance s_0^* is given by [5, 69]

$$s_0^* = \left(\frac{\mu(1+\nu)bd_p}{8\sigma_a\pi(1-\nu)}\right)^{1/2}, \tag{42}$$

and in this model the glide velocity v_{skd} of the dislocations becomes,

$$v_{skd} = \tfrac{1}{4}J_{sk}s_0^*d_p, \tag{43}$$

where J_{sk} is the single nucleation rate given by

$$J_{sk} = \frac{\nu_D bd_p\sigma_{exc}}{k_BT}\exp\left(-\frac{E_m + F_k'}{K_BT}\right). \tag{44}$$

Note that this expression is similar to the nucleation rate of double kinks except that the energy of activation for the formation of the kink is now F_k' instead of $2F_k'$. Numerical calculations show that if the thickness of an uncapped layer is sufficiently large, double kinks also form. As the thickness increases, the rate of nucleation of double kinks also increases and beyond a certain critical thickness, motion of dislocations by formation of double kinks dominates even for the uncapped layer. The thickness at which the transition from single kink to double kink nucleation takes place depends on the strain ϵ in the epilayer. It is ~1 μm for $\epsilon = 0{\cdot}2\%$ and ~200 Å for $\epsilon = 1\%$.

5.2. *Experimental results*

Dislocation velocities in GeSi strained layers have been measured by three groups: Houghton [67, 74, 75], Tuppen and Gibbings [68] and Hull *et al.* [69]. In all three cases strained GeSi epilayers were grown by MBE at temperatures between 450 and 550°C. Immediately after growth, the concentration of misfit dislocations in the layers was small. The layers were virtually pseudomorphic and were strained. The thicknesses and compositions of the epilayers were such that they were metastable. Epilayers with thicknesses between 0·04 and 3 μm and values of x between 0 and 0·4 were investigated. The layers were annealed at temperatures between the growth temperature and 900°C. Measurements were made on both capped and uncapped epilayers.

Hull *et al.* [69] annealed the epilayers *in situ* in a JEOL 2000FX transmission electron microscope using a Gatan single-tilt heating goniometer. The dislocation motion was observed and recorded with a video. The propagation velocity was determined from the video recordings. Tuppen and Gibbings [68] studied ~1 cm square samples prepared from larger epilayers by scribing and cleaving along ⟨110⟩ directions. The damaged edge regions of these samples acted as highly efficient sources of dislocations. Very high quality epilayers were selected for the experiments so that nucleation at other sites was minimized. During the annealing process, dislocations originate at the damaged region and propagate towards the centre. In many cases a scratch line was also drawn through the centre of the layer along a ⟨110⟩ direction using a diamond tipped scribing tool. This scratch line acts as an

Fig. 14

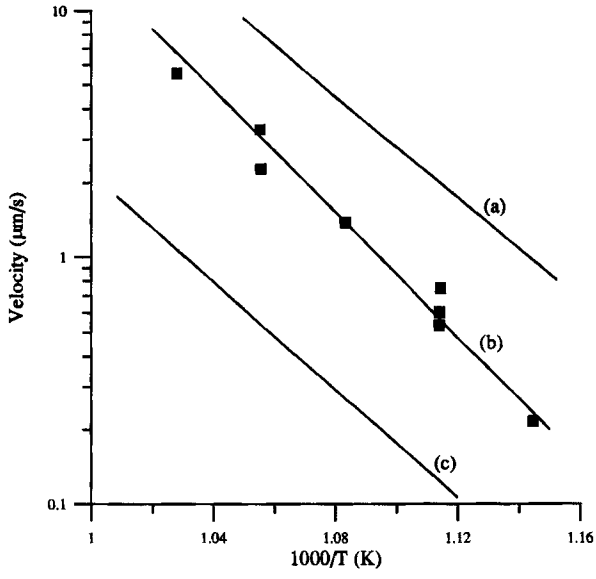

Dislocation velocity versus $1/k_BT$ for a 0·06 μm $Ge_{0.171}Si_{0.829}$ layer with 0·38 μm capping layer. Line (*a*) shows the values of V_∞, line (*b*) is the value corrected for small length of the dislocation line and solid square symbols show the experimental data. Line (*c*) represents the calculated values of the velocity if the dislocation is assumed to penetrate the capping layer up to the free surface [68].

additional source of dislocations. The dislocation structure was monitored after successive anneals by etching the samples with Schimmel etch and observing the defects by Nomarski optical microscopy. Nomarski micrographs reveal an etch pit at the end of each misfit dislocation line due to the threading arm of the dislocation which terminates at the free surface. Houghton [67, 74, 75] used transmission electron microscopy (TEM), Nomarski microscopy and other techniques to reveal the dislocation structure after successive anneals.

Typical results obtained by Tuppen and Gibbings [68] are shown in figure 14. The values calculated using Louchet's model are also shown both for the large thickness limit and for the actual thickness of the layer used. Agreement of the experimental results with the theory is quite good. Figure 14 also shows that the dislocations did not penetrate the cap.

Hull *et al.* [69] measured the glide velocity of dislocations in a thin (1000 Å) uncapped $Ge_{0.15}Si_{0.85}$ layer and compared it with the predictions of the double and the single kink models. As expected, the experimental results agreed with the single kink model.

In general the dislocation velocity in II–VI and III–V semiconductors is much larger than in Si. Recently Sumino and Yonenaga [80] have reviewed the dislocation velocities in (unstrained) Si, GaAs and InP. The velocities of dislocations for these semiconductors are plotted in figure 15. Note that, as is well known, the velocity of α dislocations (in which the extra plane terminates in group III elements) is larger than that of β dislocations (where the extra plane terminates in group V elements).

The velocity of dislocations has not been studied as extensively in $In_xGa_{1-x}As$ as in Ge_xSi_{1-x} strained layers. Bonar *et al.* [81] studied 200 Å thick capped $In_xGa_{1-x}As$

Fig. 15

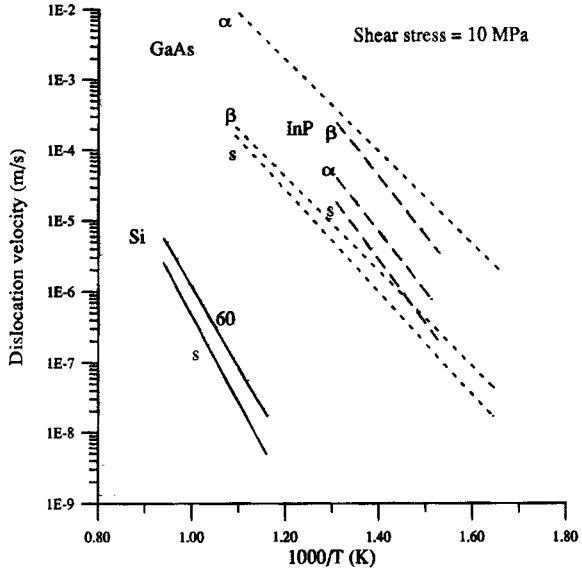

Comparison of dislocation velocities under a shear stress of 10 MPa in undoped silicon, GaAs and InP plotted against temperature. Symbols, s, α and β dislocations; 60 indicates 60° dislocations [80].

layers grown by MBE at 450°C. They estimated that the dislocation velocity was $\sim 1\ \mu m\ s^{-1}$ at 450°C and tens of $\mu m\ s^{-1}$ at 600°C. Paine *et al.* [82] studied capped layers of $In_xGa_{1-x}As$ with different concentrations of In. They found that the dislocation velocity was $1{\cdot}1\ \mu m\ s^{-1}$ at 800°C. Unfortunately the concentration of In in this sample was not quoted. The low velocity was attributed to the interaction of the moving threading dislocations with perpendicular misfit dislocations.

§ 6. Nucleation, multiplication and blocking

6.1. *Nucleation*

The homogeneous nucleation of dislocation loops at the surface of semiconductor strained layers has been studied by many authors [5, 70, 71, 83] (extensive lists of references are given in these papers). The total energy of the loop can be written as [41, 42, 71],

$$E_{\text{total}} = E_{\text{loop}} - E_{\text{strain}} \pm E_{\text{step}}. \tag{45}$$

Here E_{loop} is the self-energy of the semicircular loop of radius R, E_{strain} is the reduction of the homogeneous strain energy due to the interaction between the loop and the misfit strain and E_{step} is the energy of the surface step created or removed by the loop. Expressions for these energies have been given by several authors [41, 42, 70, 71, 83] and are somewhat different but give essentially the same numerical values. The total energy of the loop increases from 0 for $R = 0$ to a maximum value E_{act}, the activation energy for nucleation. The maximum occurs at $R = R_c$, the critical radius of the loop. As the radius increases beyond R_c, loop energy decreases and it grows at a rate determined by the velocity of the dislocations until it reaches the interface. After this, its threading arms move apart depositing the

Fig. 16

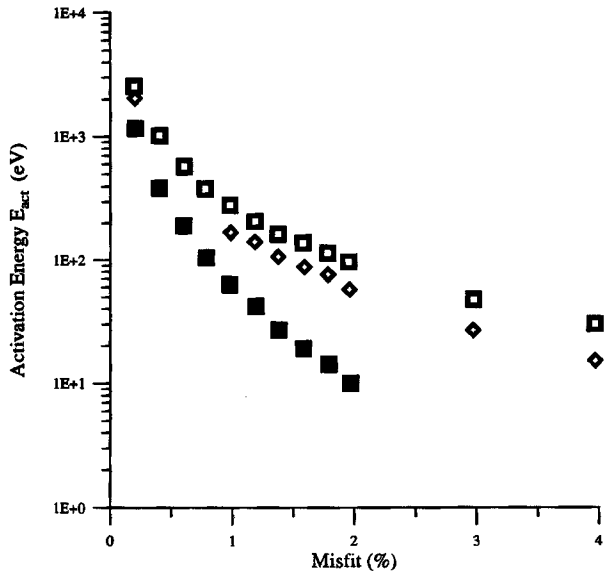

Energies E_{act} of a semicircular surface loop in a strained semiconductor layer are plotted as a function of misfit f_m. Filled squares: $\rho_c = 8/e^2 \approx 1$, diamonds: $\rho_c = 4$ and open squares: $\rho_c = 4$ but neglecting the surface energy term [71].

misfit dislocation at the interface (see figure 7). The rate of nucleation is generally assumed to be proportional to $\exp(-E_{act}/k_B T)$. The expression for E_{act} is [41, 42]:

$$E_{act} = \frac{\mu b^2 R_c (2-\nu)}{8(1-\nu)} \left[\left\{ 1 + \ln\left(\frac{\rho_c R_c}{b} \right) \right\} - \frac{8\pi R_c \epsilon (1+\nu)}{3b(2-\nu)} + \frac{16\sigma_s}{\mu b} \frac{1-\nu}{2-\nu} \right], \quad (46)$$

where

$$R_c = \frac{3b(2-\nu)}{16\pi(1+\nu)} \left[\left\{ 2 + \ln\left(\frac{\rho_c R_c}{b} \right) \right\} + \frac{16\sigma_s}{\mu b} \frac{1-\nu}{2-\nu} \right]. \quad (47)$$

Here ρ_c is the core parameter already introduced in section 2.4 and σ_s is the surface tension of the layer, which is commonly set equal to $\mu b/8$. The calculated values of E_{act}, shown in figure 16 [71], show that E_{act} decreases with increase in f_m. The contribution of surface energy and the value of the core parameter ρ_c have a large effect on the values E_{act}. Generally $\rho_c = 1$ is used for metals and $\rho_c = 4$, for covalent semiconductors [71, 77]. For $f_m = 0{\cdot}02$, $E_{act} \sim 10$ eV for $\rho_c = 8/e^2 \approx 1$ and >100 eV for $\rho_c = 4$ (see figure 16). Similar values of the energy of activation have been calculated for the InGaAs/GaAs system [84]. The values for the energy of activation for $\rho_c = 4$ are so large that homogeneous nucleation is very unlikely to occur for any reasonable values of the misfit parameter. In most cases the observed values of the activation energies are much lower and have been attributed to heterogeneous nucleation. It has been known for many years that point defects and their clusters lower the activation energy dramatically [41, 42] and act as efficient sources for the nucleation of dislocations. Little theoretical work on heterogeneous nucleation in semiconductor strained layers has been done, presumably because many unknowns are involved and the process is very complex.

It should be pointed out that the loop can nucleate only if $h > h_d$, where

$$h_d = R_c \cos \phi, \tag{48}$$

and ϕ is the angle between the surface and the normal to the slip plane [41, 42]. If $\rho_c \approx 1$, values of h_c calculated using (32) and h_d using (48) are nearly the same. Sufficient thermal energy is also needed for the loop to attain the critical radius.

Several experimental studies of the nucleation of dislocations in strained semiconductor layers have been made. In most cases nucleation was observed at much lower temperatures than those predicted by the calculations for homogeneous nucleation. Interfacial defects such as oxide contamination [85] and β-SiC particles [83] were found to be efficient sources of dislocations. Higgs *et al.* [86] found that copper contamination of the GeSi strained layers in trace amounts increased the strain relaxation rate considerably. Similarly Hull *et al.* [87] observed that the rate of strain relaxation was enhanced in samples in which defects were introduced by ion implantation.

A low energy of activation has also been attributed to 'intrinsic' sources. Eaglesham *et al.* [71] found a new regenerative source, designated as the diamond defect (because its shape resembles diamond), that can generate dislocations of more than one **b** at low misfits in GeSi strained layers. The authors suggested that the defect is intrinsic and is probably produced by precipitation of interstitials. Perovic and Houghton [83] suggested that nucleation takes place at atomic ledges trapped at the interface between substrate and epilayer. They used $\rho_c = 0{\cdot}6$ and $E_{act} \approx 0$ for $f_m = 0{\cdot}015$ to interpret their experiments on GeSi strained layers. Hull and Bean [70] observed relatively long 60° dislocations in 2500 Å $Ge_{0.15}Si_{0.85}$ layers annealed at 700°C. 350 Å layers with 25% Ge concentration, annealed at 800°C, showed 90° dislocations. The number of dislocations increased with an increase in temperature of annealing. Hull and Bean [70] argued that in GeSi alloys, the activation energy should be lowered on two accounts. Preferential accumulation of Ge near the core (in the compressed layers) can substantially reduce the non-elastic core energy and they suggested that the value of ρ_c should be reduced from 4 to 2 to account for this. Furthermore, due to random fluctuation of Ge concentration, the activation energy is lowered in regions where local Ge concentration is high. For $x \geqslant 0{\cdot}25$, the activation energy is sufficiently lowered that dislocations can be introduced by homogeneous nucleation at the surface. For lower Ge concentrations, the 'intrinsic defect' sources discussed above [71, 83] are needed to facilitate the nucleation.

Nucleation of dislocations also involves their propagation and it is not easy to determine separately the nucleation energy and the activation energy for motion. In another paper, Hull *et al.* [88] interpreted their annealing experiments assuming a constant rate of nucleation. Since the activation energy increases as strain decreases, Gosling *et al.* [72] reinterpreted the observed data of Hull *et al.* [88] assuming that the activation energy varies as $1/|\epsilon|$ and using an Arrhenius-type expression for the rate at which the number of dislocations increases by nucleation [72]:

$$J_{nuc} = J_0 \exp(-\lambda/k_B T|\epsilon|), \tag{49}$$

where J_0 is a constant pre-exponential frequency factor per unit area and $\lambda/|\epsilon|$ is the activation energy. Gosling *et al.* [72] obtained $\lambda = 0{\cdot}003$ eV. The initial misfit strain in the samples of Hull *et al.* [88] is $f_m = 0{\cdot}01$ for which $\lambda/|\epsilon|$, the activation energy

for nucleation, is 0·3 eV. This work of Hull *et al.* [88] is discussed in more detail in section 7.

Recently LeGoues *et al.* [89] have measured the strain relaxation in GeSi strained layers with an intermediate graded layer grown on a Si surface with a miscut away from the (100) surface. The authors showed that the relaxation was nucleation limited and obtained $E_{act} = 5{\cdot}3$ eV. It is not clear what value of ϵ should be used to interpret these experiments, nor do we know whether the nucleation was homogeneous or heterogeneous.

6.2. *Multiplication*

Whether or not multiplication of dislocations plays a significant role in annealing and stress relaxation experiments depends strongly on the experimental conditions and sample history. In their extensive experimental investigations, Hull *et al.* [71, 87, 88] found no evidence of multiplication and in the analysis and interpretation of their results, they neglected multiplication altogether (see section 7). However, results of other authors provide evidence for its importance [73, 85, 90, 91].

In the experiments of Tuppen *et al.* [85], initially dislocations nucleated at heterogeneous sources and a large number of dislocations were produced on closely spaced {111} planes. As this number increases, the local stress decreases and the sources become ineffective. The sample is now divided into regions where the strain has relaxed more or less completely and others, where the strain is still quite large. If the annealing continues, relaxation spreads across the whole sample. Tuppen *et al.* [85] described a multiplication process whereby the existing dislocations multiply and lead to relaxation of the strain in regions away from the nucleation sources. LeGoues *et al.* [89, 91] prepared high quality GeSi strained layers and performed *in situ* and *ex situ* annealing experiments. The observed relaxation of the strain in their samples could only be explained by assuming that multiplication of precursor existing dislocations occurs through a mechanism similar to the Frank–Read mechanism. Alternatively the Hagen–Strunk mechanism discussed in [71, 84, 92a, b] operates when two dislocations meet each other at right angles. Multiplication of dislocations by this mechanism has been observed in both GeSi strained layers [71] and InGaAs strained layers [84]. It operates efficiently only if neither the layer thickness nor the misfit are very large. Doubts have also been expressed as to whether this mechanism was really operative in some of these experiments [84, 71]. Other methods of multiplication have been discussed in [5, 93].

The rate of increase of the number of dislocations by multiplication, J_{mult}, has been discussed by several authors. According to the phenomenological models of Dodson and Tsao [73] and of Nix *et al.* [90] the rate is given by

$$J_{mult} = N_m \delta v_d \tag{50}$$

where N_m is the number of mobile threading dislocations and δ is a breeding factor. Nix *et al.* [90] used a constant breeding factor $\delta = \delta_0$ whereas Dodson and Tsao [73] used

$$\delta \propto \sigma_{exc}. \tag{51}$$

If the Hagen–Strunk mechanism is operative [72],

$$J_{mult} = \frac{1}{2}\frac{dN_i}{dt} P_{mult} = -\frac{(\epsilon + f_m) n_m v_d}{2 b_{eff}} P_{mult}, \tag{52}$$

where the number of intersections is given by

$$N_i = \frac{L^2}{4A}. \tag{53}$$

P_{mult} is the probability that an interaction of the appropriate type leads to a multiplication event. It depends on the lattice mismatch and the thickness of the epilayer. In the mechanisms proposed by LeGoues *et al.* [91] and Lefebvre *et al.* [93], a single annihilation event leads to a regenerative source, similar to the Frank–Read source. In these mechanisms, the multiplication rate is of the form [72]

$$J_{mult} = \tfrac{1}{4} N_i J_0 \exp(-\lambda/k_B T|\epsilon|) = \frac{1}{4}\left(\frac{\epsilon + f_m}{b_{eff}}\right)^2 J_0 \exp(-\lambda/k_B T|\epsilon|), \tag{54}$$

where, as previously, $\lambda/|\epsilon|$ represents an activation energy, and J_0 is a frequency factor per unit area.

6.3. *Blocking*

A misfit dislocation is produced by a moving threading dislocation in a strained layer as illustrated in figure 17. The free surface of the layer is at $x_2 = h$ and the substrate–layer interface is at $x_2 = 0$ and the glide plane of the dislocation is inclined at an angle α to the x_2-axis. The coordinates of the bottom of the threading dislocation are $(x_1, x_2) = (x, y)$. A misfit dislocation is formed at a height y above the interface. A misfit dislocation shown running along the x_3-axis will interact and impede the motion of the threading dislocation if the two dislocations have the right kind of Burgers vectors. There are four pairs of strain relieving Burgers vectors, only one of which causes significant blocking of the moving dislocation. The probability

Fig. 17

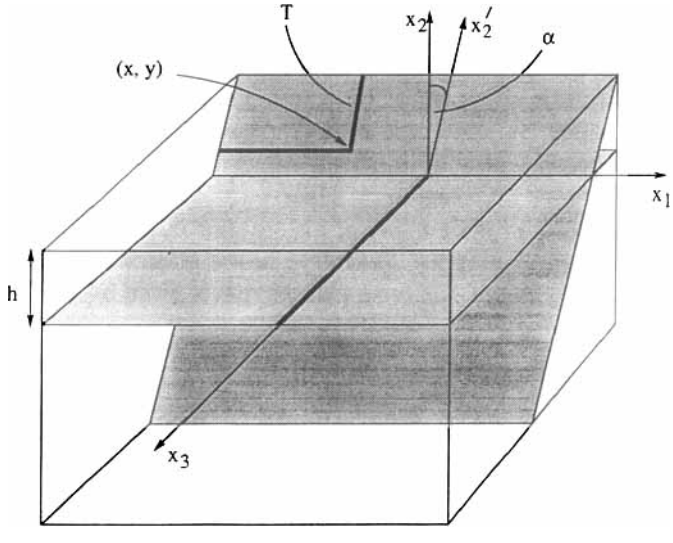

Schematic illustration of the motion of a threading dislocation through a strained layer, illustrating the coordinate system used. Also illustrated is a perpendicular misfit dislocation along the x_3-axis, with which the threading dislocation interacts [72].

Fig. 18

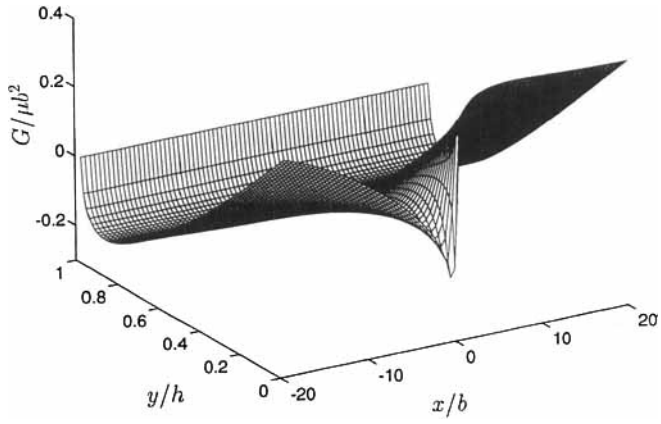

Surface plot of the driving force $G(x, y)$ on a threading dislocation in a strained layer (lattice-mismatched by 2% relative to its substrate, and of thickness 110 Å) as it approaches a perpendicular misfit dislocation, with which it interacts. The Burgers vectors of the two dislocations has been chosen so that the interaction is repulsive [72].

that the dislocation interaction can impede the motion of the threading dislocation is therefore 1/4.

We now calculate the rate at which the number of mobile dislocations is decreased by the blocking. Let the Burgers vector of the perpendicular misfit dislocation be **a**, defined relative to a line direction chosen positive in the direction of the positive x_3-axis, then the local net force $G(x, 0)$ acting on the threading dislocation, including the interaction with the orthogonal misfit dislocation, is given to a very good approximation by [72],

$$G(x,y) = -E^{s}(h-y) + \mu b\left(\frac{1+\nu}{1-\nu}\right)|\epsilon|(h-y) + \frac{2{\cdot}5\mu b^2}{2\pi(1-\nu)}\left\{\frac{1+\nu}{4}\ln\left(\frac{x^2+y^2}{x^2+h^2}\right)^{1/2} + \frac{1-3\nu}{2(2)^{1/2}}\left[\tan^{-1}\left(\frac{x}{y}\right) - \tan^{-1}\left(\frac{x}{h}\right)\right]\right\}. \tag{55}$$

Here $E^{s}(h-y)$ is the energy E_{D}^{∞} defined in equation (13), with $h-y$ substituted for h and the term involving $2{\cdot}5\mu b^2$ is the force due to the interaction with the perpendicular misfit dislocation. The force $G(x, y)$ calculated for $f_m = 0{\cdot}02$ and thickness of the layer $h = 110$ Å is shown in figure 18. It is seen from the figure that there is a saddlepoint in the plot. The saddlepoint force G^* is a minimum with respect to x and a maximum with respect to y. In the case considered, $G^* > 0$ and the threading dislocation will cross over depositing a misfit location at a height near the saddle point. If $G^* < 0$, blocking will occur provided the Burgers vectors of the two dislocations are of the right type. If other dislocations are present in the layer, we replace the mismatch strain $-f_m$ in all equations by the mean strain in the layer, ϵ, given by (11).

The saddlepoint values of x and y are given by

$$y = \frac{(1-3\nu)(2)^{1/2}x^2 - (1+\nu)xh}{(1-3\nu)(2)^{1/2}h + (1+\nu)x}. \tag{56}$$

$$[b_e^2 + (1-\nu)b_s^2]\frac{(1-3\nu)(2)^{1/2}h + (1+\nu)x}{(1-3\nu)(2)^{1/2}(h^2-x^2) + 2(1+\nu)xh} - 4\pi b(1+\nu)|\epsilon| - 2{\cdot}5b^2\frac{[(1-3\nu)(2)^{1/2}h + (1+\nu)x]h}{2(x^2+h^2)x} = 0. \tag{57}$$

The smallest negative solution of equation (57) corresponds to the saddlepoint and is in the region of $x^* = -2b$. The corresponding value of y^* can be obtained from (56). Using these values of saddlepoint coordinates, the sign of G^* is determined from equation (55). As stated above, if $G^* > 0$ then no blocking occurs for the given combination of ϵ and h. If $G^* < 0$ then blocking will occur if the pair of Burgers vectors $(\mathbf{a}, \mathbf{b})$ are of the right type.

The number of dislocations blocked per unit time, J_{block} is given by

$$J_{\text{block}} = \frac{dN_i(t)}{dt}P(t). \tag{58}$$

Here $N_i(t)$ is the total number of interactions given by equation (53) and $P(t)$ is the blocking probability. $P(t)$ is 1/4 if $G^* < 0$ and 0 otherwise. Differentiating equation (53) and using (65), (11) and (67), (58) can be written as [72]:

$$J_{\text{block}} = -\frac{(\epsilon + f_m)N_m v_d}{b_{\text{eff}}}\frac{H(-G^*(\epsilon,h))}{4}, \tag{59}$$

where the Heaviside step function

$$H(x) = \begin{cases} 1 & \text{if } x > 0 \\ 0 & \text{otherwise.} \end{cases}$$

If the propagating dislocation interacts with a closely bunched cluster of N misfit dislocations with identical Burgers vectors, the interaction force is multiplied by a factor N [94].

§ 7. Annealing and strain relaxation

7.1. *Excess stress and the Dodson–Tsao equation*

Dodson and Tsao (see the review [73] for a discussion of Dodson–Tsao theory) modified the theory of plastic flow [95] so that it can be used to model strain relaxation in epilayers. Using equations (36), (50) and (51), we obtain the Dodson–Tsao equation [44],

$$\frac{d\gamma}{dt} = C_1\mu^2(f_m - r(h) - \gamma)^2(\gamma + \gamma_0) \tag{60}$$

where

$$\gamma(t) = -\frac{b_1}{p(t)} = f_m - \epsilon(t), \tag{61}$$

$$r(h) = \frac{\mu b\cos\alpha(1-\nu\cos^2\beta)}{4\pi h(1-\nu)}\ln\frac{\rho_c h}{b}. \tag{62}$$

Fig. 19

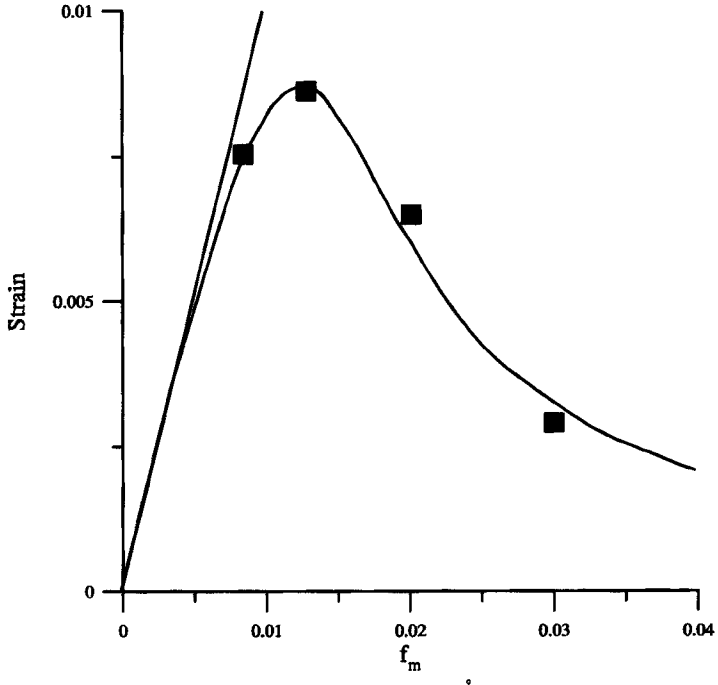

Strain in the epilayers as a function of f_m for $h = 500$ Å. solid curve: theory including the interactions; solid symbols, experimental data [96] and straight line: strain in a pseudomorphic layer [44].

$$C_1 = \text{constant} \exp\left(-\frac{E_v}{k_B T}\right), \tag{63}$$

and γ_0 is the background source which helps in starting the multiplication process. If the annealing is done after growth and h is constant, equation (60) can be integrated analytically [44], to give

$$t = \frac{1}{C_1 \mu^2 (f_m - r - \gamma_0)^2}\left[\ln\frac{\gamma_0 + \gamma}{f_m - r - \gamma} + \frac{f_m - r + \gamma_0}{f_m - r - \gamma} - \ln\frac{\gamma_0}{f_m - r} - \frac{f_m - r + \gamma_0}{f_m - r}\right], \tag{64}$$

where we have used r for $r(h)$ for convenience. These solutions cannot be used if h does not remain constant during the strain relaxation. To model strain relaxation during growth, a numerical integration is necessary.

The effect of the interactions on $r(h)$ and therefore on plastic flow is quite significant [44]. If interactions are included, an analytical solution for strain relaxation cannot be obtained.

Dodson–Tsao theory has been compared with the experiments of Bean *et al.* [96] in both cases, i.e. using the earlier theory [73] and including the interactions correctly [44]. In Bean's experiments, the epilayers were grown by MBE at 550°C at a growth rate of 5 Å s^{-1} [96]. The time for which plastic flow occurs and gives rise to strain relaxation was assumed to be dominated by a cool down period of approximately 1000 s. C_1 and γ_0 were assumed to be adjustable parameters. The fit of Bean's data with the theory (including interactions [44]) for $h = 500$ Å is shown in figure 19. The

Table 2. Parameters C_1 and γ_0 for $h = 500$ Å obtained by fitting the plastic flow theory with interactions (Jain *et al.* [44]) and earlier theory (Dodson [73]) to the experimental data.

	$C_1\mu^2$ (s^{-1})	γ_0
Dodson [73]	46	3×10^{-5}
Jain *et al.* [44]	14	9×10^{-4}

values of the constants γ_0 and C_1 obtained with interactions [44] and using approximate theory [73] for $h = 500$ Å are compared in table 2. The effect of interactions on the values of the parameters is large. C_1 is a material parameter and its temperature dependence determines the energy of activation of the glide velocity. Correct values of this parameter are required for predicting values of strain relaxation under different experimental conditions and for determining the stability of the strained layer heterostructure devices. It is necessary to include the effect of an irregular distribution of dislocations in interpreting these experiments in detail and to obtain more reliable values of the material parameters.

Jain *et al.* [44] found that Nix *et al.*'s theory [90] with a constant breeding factor δ could not account for the above experiments. Similarly the Dodson–Tsao equation could not be fitted to the experimental data analysed by Nix *et al.* [90]. These theories neglect nucleation and blocking of the dislocations and are highly phenomenological.

7.2. *Improved theory of strain relaxation*

The total length L of misfit dislocations is given by the following differential equation

$$\frac{dL}{dt} = N_m v_d, \tag{65}$$

where N_m is the number of mobile threading dislocations. In writing this equation we have assumed that the numbers of threading and misfit dislocations are equal. This is true when the threading dislocations are the substrate dislocations as shown in figure 7 (*c*). If the dominant process is nucleation of surface loops as shown in figure 7 (*a*) and 7 (*b*), the number of mobile threading dislocations is twice as large as that of misfit dislocations and there will be a factor 2 on the right hand side of equation (65). The rate of change of the number of mobile threading dislocations is given by [72]

$$\frac{dN_m}{dt} = -J_{block} + J_{nuc} + J_{mult}, \tag{66}$$

and the dislocation spacing p is given by

$$\frac{1}{p} = \frac{L}{2A}, \tag{67}$$

where A is the surface area of the device. Using (11) and (65), we may write (67) as

$$\frac{d\epsilon}{dt} = -\frac{b_1 N_m v_d}{2A}. \tag{68}$$

The dislocation velocity v_d is given by v_∞ in equation (41). The expressions for v_d, J_{block}, J_{nuc} and J_{mult} involve ϵ and N_m. Equations (66) and (68) provide a pair of coupled first order differential equations that may be solved to calculate strain

relaxation or the number of dislocations as a function of annealing time and temperature.

7.3. *Interpretation of annealing experiments*

Hull *et al.* [88] performed a series of growth and annealing experiments on 350 Å $Ge_{0.25}Si_{0.75}$/Si(100) strained layers. The layers were grown by MBE at 550°C at a rate of 3 Å s^{-1} and then successively annealed for 240 s at each of six temperatures in the range 550°C and 850°C. The threading dislocation concentration and average misfit dislocation spacing were measured. Gosling *et al.* [72] found that the experimental results can be reproduced only if it is assumed that blocking occurs from the very beginning and if misfit dislocations are present in clusters of two to three with identical Burgers vectors. The formation of dislocations in clusters with identical Burgers vectors is supported by experimental evidence. Nucleation of dislocations occurs at fixed heterogeneous sources which generate several dislocations very close together [41, 42, 84, 85]. Assuming these dislocations originate from the same source, they will have identical Burgers vectors [84]. Since each interaction involves three misfit dislocations, the number of intersections N_i, given by (53), is reduced by 3. For 60° dislocations, equation (59) for the blocking rate becomes [72]

$$J_{\text{block}} = \frac{|\epsilon + f_m| N_m v_d}{6b}.$$

Hull *et al.* [88] have mentioned that there was no evidence for multiplication events, and therefore J_{mult} was neglected. J_0 and λ were used as adjustable parameters.

Taking $\epsilon = -f_m = 0{\cdot}105$ and the observed density of threading dislocations as 10^3 cm^{-2} at time $t = 0$, (66) and (68) were integrated [12] numerically. Gosling *et al.* [72] obtained a reasonable fit with experiment with $J_0/A = 1{\cdot}3 \times 10^{10}$ m^{-2} s^{-1} and $\lambda = 0{\cdot}0032$ eV. Calculated and experimental values of threading dislocation density are shown in figure 20. Note that N_t includes threading dislocations that have been blocked as well as those that are mobile. This value of λ corresponds to a nucleation activation energy of 0·3 eV for $f_m = 1\%$. The activation energy is low and suggests that nucleation was heterogeneous. There is agreement between theory and experiment within a factor two or better over almost the whole temperature range. In view of the fact that the distribution of dislocations is highly irregular, that not all observations are made on exactly the same sample and that there are inherent uncertainties associated with the measurements, this agreement is regarded as satisfactory. The agreement between theoretical and experimental values of mean dislocation spacing $\bar{p}$ was similar.

Strain relaxation measurements in $In_xGa_{1-x}As$ strained layers have been made by Paine *et al.* [82]. The layers, capped, 236·4 nm thick and with 4 values of x, (= 0·05, 0·1, 0·19 and 0·22) were grown at 520°C. Two of the layers with $x = 0{\cdot}1$ and $x = 0{\cdot}19$ were annealed for 120 s at each of the 5 temperatures, 800, 850, 900, 950 and 1000°C, respectively. After each anneal the spacing between the dislocations was measured by TEM. The measured values of spacing are shown in figure 21. Theoretical analysis of these results to extract values of nucleation activation energy and dislocation velocity has not yet been undertaken. Bonar *et al.* [81] measured the dislocation velocity and dislocation structure in capped $In_xGa_{1-x}As$ strained layers. For $x > 0{\cdot}4$ pure edge dislocations with $\mathbf{b} = (a/2)\langle 101\rangle$ gliding on {101} plane were observed. High stresses due to the large In concentration and the large value of Schmid factor for the edge dislocations were responsible for this new glide system.

Fig. 20

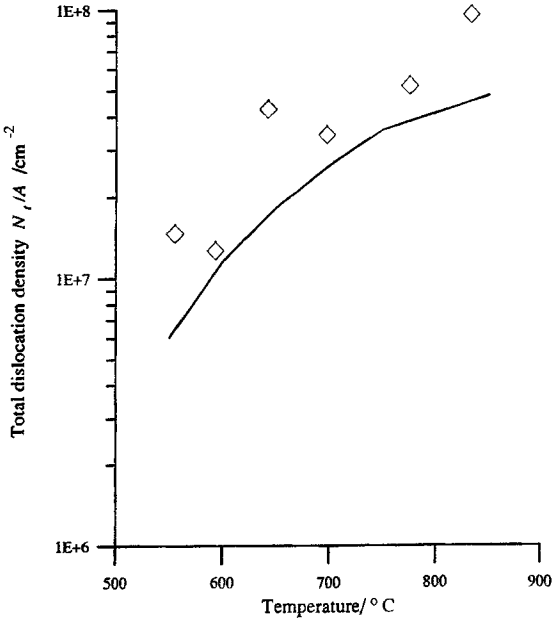

Theoretical values of threading dislocation density N_t/A compared with experimental values of Hull *et al.* [85] for a 350 Å $Ge_{0.25}Si_{0.75}$/Si(100) layer grown at a rate of 3 Å s^{-1} at 550°C and then successively annealed for 240 s at each of the temperatures for which a data point is shown [72].

Fig. 21

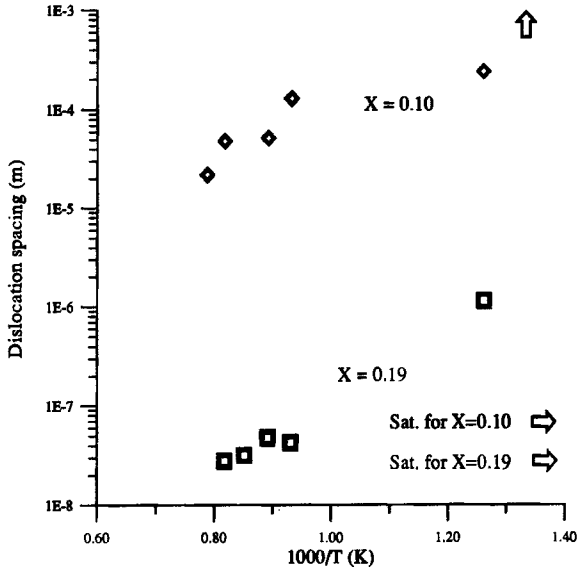

The average dislocation spacing versus inverse absolute temperature. The observed spacing immediately after growth at 480°C (marked by vertical arrow) is shown on the extreme right. Horizontal arrows indicate the saturation spacing for pure edge dislocations. For 60° dislocations this spacing will be reduced by a factor 1/2 [80].

§ 8. Metallic systems

The theory developed in the previous sections can equally well be applied to metallic systems, but because the presence of dislocations is expected to have a less important effect on the properties than in semiconductors far less detailed work has been performed to test the theory with well controlled epitaxial systems. The qualitative features of the theory were confirmed experimentally in the 1960s and the work of Jesser and Matthews [97] with cobalt films on copper is typical. A single crystal film of copper was prepared by evaporating the metal onto a cleaved face of an alkali halide. Cobalt films were then deposited of various thicknesses and the structure examined with an electron microscope. When the cobalt was deposited on the copper at room temperature it initially formed a face centred cubic strained structure which was lattice matched to the copper lattice. When the film thickness exceeded 20 Å misfit dislocations were observed and on increasing the thickness these became more numerous and the crystal structure became in some regions closer to hexagonal close packed.

This is qualitatively in excellent accord with the theory. Experiments were also performed depositing the cobalt onto the copper substrate at 350°C. The growth was then in the form of lattice matched centred islands which grew up to 300 Å in size.

After this initial progress there have been few detailed studies of the critical thickness for metal systems. Many metal systems are grown by sputtering techniques when the crystallites in the film are relatively small and the boundaries between the crystallites prohibit detailed quantitative studies. Even when metal layers are grown with molecular beam epitaxy their crystalline quality is much poorer than that of the semiconductors and so we are unaware of detailed studies of h_c and the behaviour of the lattice parameter with thickness.

A recent experiment was performed to study the growth of Cu(001) on Fe(001) surface using X-ray diffraction [64], figure 22 shows the Cu in-plane spacing as a

Fig. 22

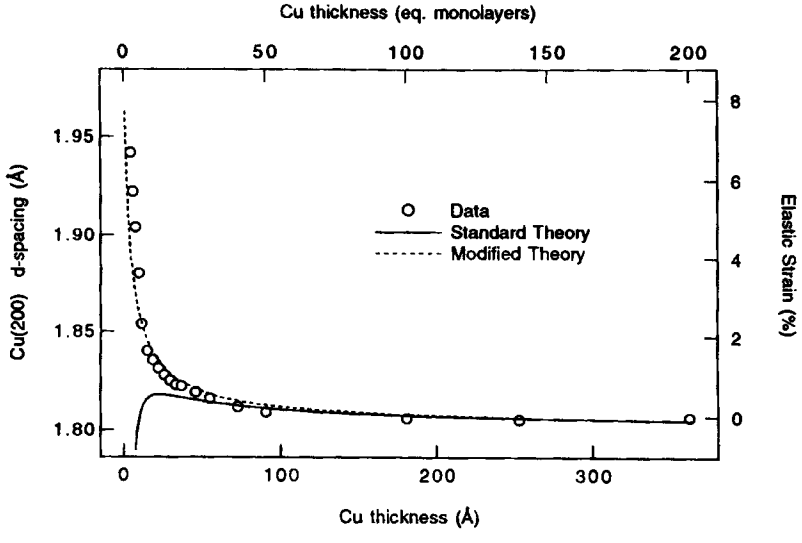

Cu d spacing against Cu film thickness for Cu grown on Fe (001) showing the in-plane strain. The lines are different theories [64].

Fig. 23

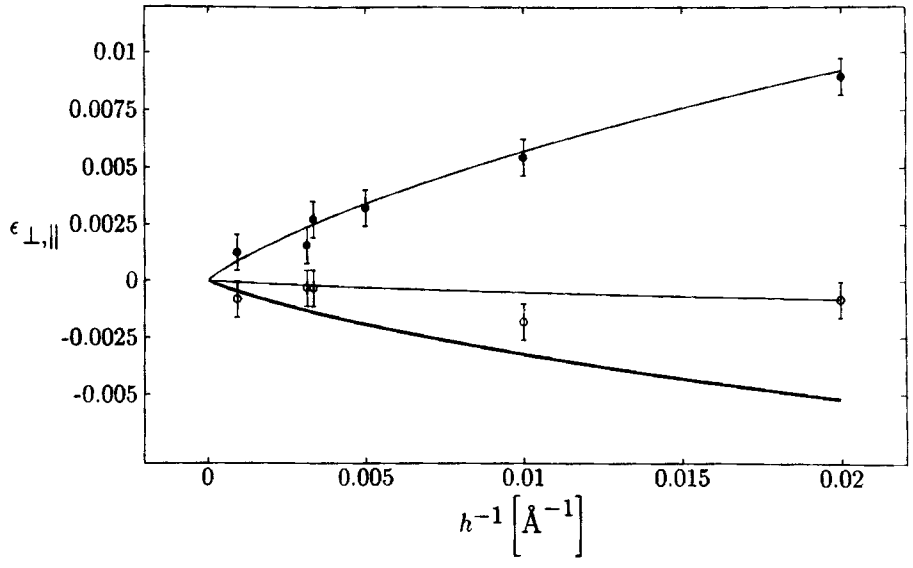

The Cr lattice parameter in-plane (solid) and out-of-plane (open) as a function of inverse film thickness grown of Nb. The thick line shows the expected out-of-plane lattice parameter calculated using Poisson's ratio [99].

function of the Cu plane thickness. The relaxation occurs for small thicknesses because the misfit strain is large, 12·1%. The dotted line is a one parameter fit to the experiment results with the standard theory modified to take account of the Peierls–Nabarro model for the dislocation core as described in section 3.1. The agreement shows that for these large strains, metastable states and relaxation are not a problem for metallic layers.

An unexpected result is that a number of magnetic thin films and parts of multilayers show an expansion of both in-plane and out-of-plane directions [98]. This is clearly inconsistent with a simple model and elasticity theory. It does therefore raise the question as to whether the dislocation theory, depending as it does on elasticity theory, can be relied upon to give correct answers for the energy of the dislocation or whether the possibility of changes in the electron density in thin metallic layers can change the properties substantially from those of the bulk.

These difficulties are illustrated by the results of X-ray measurements of Cr films deposited on Nb [99]. In figure 23, we show the lattice parameters obtained within the Cr film and between the different atomic layers in the Cr film. The latter increases with increasing film thickness as expected, to take up the misfit strain. The former is almost constant, however, in contrast to the prediction of elasticity theory shown by the heavy solid line. The dotted lines are calculated on the basis of a simplified form of the theory outlined in sections 2 and 3, but the parameters have been fitted to the data and so only the qualitative behaviour is significant.

An interesting new development [100–102] to the theory has been its application to describing the behaviour of ferroelectric films. When these films become ferroelectric the crystal structure distorts to say a tetragonal form from a cubic form and so different directions will have different misfit strains. This could then alter the

density of dislocations in different directions, and hence influence the ferroelectric domain structure of the film. These are clearly important considerations in the applications of these materials and more detailed experimental studies are needed of the effects.

§ 9. Structure of absorbed monolayers

The concept of misfit dislocations has played an important role in the understanding of the structure of absorbed monolayers. Because these systems are two-dimensional, their properties differ considerably from those of the three-dimensional systems discussed above because of the greater importance of fluctuations in lower dimensions. Many of the experiments have been performed by studying gases absorbed onto the planar surfaces of pyrolytic graphite.

Although many experimental techniques have been used to study these systems, the application of X-ray techniques using synchrotron sources has been especially fruitful as the resolution and wavelength of X-rays are well matched to the parameters of the physical structures. We shall use a variety of different experiments to illustrate the basic results following a very useful review [103].

9.1. *Commensurate–incommensurate transitions*

The Hamiltonian for a one-dimensional system comprising a line of absorbed atoms connected by harmonic forces and subjected to a harmonic substrate potential has the form

$$H = \sum_n \left\{ \frac{K}{2}(z_{n+1} - z_n - a')^2 + V\left[1 - \cos\left(\frac{2\pi z n}{a}\right)\right]\right\}, \tag{69}$$

where K is the spring constant, the natural spacing is a' and the substrate potential V has a natural spacing a. If a' and a are not too different the solution to this Hamiltonian has the form of nearly commensurate regions of absorbed atoms separated by discommensurations or dislocations. The Hamiltonian is solved by writing in terms of the average lattice constant $\bar{a}$, as

$$z_n = n\bar{a} + \frac{\bar{a}}{2\pi}\phi_n,$$

and transforming to the continuum limit when

$$H = \int \left[\frac{K\bar{a}^2}{8\pi^2}\left(\left(\frac{\mathrm{d}\phi}{\mathrm{d}n}\right) - \delta\right)^2 + V(1 - \cos\lambda\phi)\right] \mathrm{d}n, \tag{70}$$

where $\lambda = \bar{a}/a$ and $\delta = 2\pi(a'/\bar{a} - 1)$. This Hamiltonian was considered numerically by Macmillan [104] and solved more elegantly by Bak and Emery [29] who showed that ϕ satisfied the sine–Gordon equation, one solution of which is the domain wall or soliton which separates regions of commensurate structure. The domain wall width is

$$d = \frac{\bar{a}}{2\pi\lambda}\left(\frac{K}{V}\right)^{1/2}.$$

The energy to create a domain wall is

$$E_1 = \left(\frac{4}{\pi d\lambda} - \delta\right)\frac{2\pi}{\lambda}, \tag{71}$$

while the interaction between two neighbouring domain walls separated by a distance $p > d$ is

$$E_2 = \frac{32}{\lambda^2 d}\exp\left(-\frac{d}{p}\right). \tag{72}$$

The total energy density of the system is then given as

$$E = \frac{1}{p}(E_1 + E_2), \tag{73}$$

where it is assumed that only nearest neighbour domain walls can interact.

The experiments allow the volume of absorbed material on the substrate to be varied so that the coverage and hence the mean spacing $\bar{a}$ changes. A domain wall structure will be formed when $E_1 < 0$ or when $\delta > \delta_c = 4/(\pi d\lambda)$ and for larger values of δ a domain wall structure is formed with a regular spacing given by

$$\frac{1}{p_s} = -\frac{1}{d}\ln\left(\frac{|E_1|\lambda^2 d}{32}\right) = -C\ln(\delta - \delta_c) \tag{74}$$

where C is a constant.

This is different from the linear dependence of $1/p_s$ on $h - h_c$ given in equation (34) because the domain walls discussed in this section do not have long range strain fields and so the form of the interaction term is $(1/p)\exp(-d/p)$ whereas for the dislocations discussed in section 2 the interactions have the form $1/p^2$.

As mentioned above one of the interests in studying two-dimensional systems is that fluctuations are very important and the above discussion has neglected any account of the fluctuations in the positions of the domain walls. These effects were first treated by Pokrovsky and Talapov [105] and then more physically by Fisher and Fisher [106]. The basic argument is that the domain wall in the absorbed film is a line and fluctuations cause this line not to be straight but to wander. The average deviation of a line of length L diverges as L increases due to the long range fluctuations, showing that their entropic effects will certainly cause the domain walls to become very close. This changes the effective interaction between two walls from the exponential form (equation (72)) to an energy proportional to T/p^2, where T is the temperature. As a result the behaviour of p_s for δ close to δ_c has the form

$$\frac{1}{p_s} \sim (\delta - \delta_c)^{1/2}. \tag{75}$$

One other effect of the fluctuations is that since the domain walls fluctuate they are not regularly spaced and the system does not have long range order. Since this incommensurate phase has a continuous broken symmetry the result is a consequence of the usual result that two-dimensional systems with a continuous symmetry do not have long range order. The specific case of a two-dimensional incommensurate phase has been discussed [106], and the results show an algebraic decay of the correlation functions. In a scattering experiment the Bragg peaks from an ordered domain wall structure occur when the wavevector transfer is given by $\delta(Q - \tau)$ with $\tau = 2\pi N/p_s$. In the incommensurate phase the delta functions are replaced by

$$S(Q) = \frac{A}{(Q - \tau)^{2-\eta}}, \tag{76}$$

Fig. 24

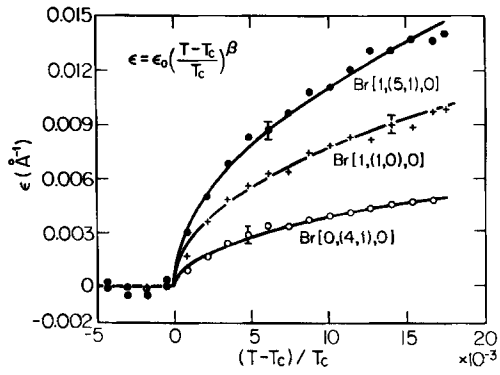

The change in wavevector at the commensurate–incommensurate transition of Br on graphite [107]. The data gives $\beta = 0{\cdot}50 \pm 0{\cdot}02$ in agreement with theory [106].

where the exponent η depends on the temperature, wavevector transfer and order of the Bragg reflection N.

These predictions have been very elegantly confirmed by X-ray scattering studies of bromine on graphite [107]. Figure 24 shows the temperature dependence of the wavevector of the peaks in the scattering. The shifts in the positions of the peaks, ϵ, are a direct measure of $1/q_s$ and the solid lines show fits to the predicted $(\delta - \delta_c)^{1/2}$ behaviour by varying the temperature which gives a linear variation in δ. The results for the exponent gave $0{\cdot}50 \pm 0{\cdot}02$ in excellent agreement with theory. The magnitude of ϵ for the different positions in reciprocal space is also in agreement with that predicted from a detailed analysis of the effect of the ordering on different Bragg peaks.

Measurements using high resolution synchrotron source techniques have also confirmed [108] the predicted algebraic form, equation (76), of the scattering instead of the normal Bragg peak form. The fluctuations do therefore destroy the long range order of the dislocation lattice. Furthermore the measured values of the exponent η confirm the predicted behaviour showing that these systems are well described by the theories [105, 106] outlined above.

The above results were all obtained for bromine intercalated onto graphite for which the incommensurate structure is described by a one-dimensional array of walls within the absorbed monolayer. The structures of monolayers of the rare gas solids Ar, Kr and Xe are more complex. For example, below a critical chemical potential a Kr monolayer forms a commensurate triangular structure with a $3^{1/2} \times 3^{1/2}$ unit cell. As the chemical potential is increased a structure incommensurate with the graphite substrate is formed. This structure has on average triangular symmetry and it was proposed that it could be described by a honeycomb network of dislocation lines within the monolayer. For temperatures between 50 and 95 K, the incommensurability, ϵ, varied with the difference in chemical potential to the power $0{\cdot}33 \pm 0{\cdot}03$ while at temperatures the transition was of first order and at higher temperatures the exponent increased [109]. Higher resolution measurements [110] showed that the scattering in the incommensurate phase was broadened, suggesting that there was no longer range order. This behaviour has been described theoretically by Coppersmith *et al.* [111] who considered the properties of the two-dimensional dislocation lattice.

Firstly they showed that the regular honeycomb lattice was unstable against the motion of the dislocations and so the lattice of dislocations was in a fluid state and long range order should not be expected. Secondly, they predicted that the commensurate–incommensurate transition should be weakly first order. At present the first of these predictions is in agreement with the experimental results but the latter prediction has not been observed experimentally.

9.2. *Two-dimensional melting*

Although there is no satisfactory understanding of melting in three dimensions, there is an elegant dislocation based theory of melting for two-dimensional layers. In two dimensions dislocations are point defects and for any temperature the dislocations are bound in pairs. Above the melting temperature the thermal energy enables the dislocation pairs to unbind and as a result the translational order is destroyed. This theory is similar to the theory of a two-dimensional XY magnet and leads to the prediction of a continuous phase transition [112–114], or phase transitions because the melting can successively and independently destroy firstly translational and then orientational order.

There have been a number of experimental studies [115] of rare gas layers on graphite but scattering experiments have found it difficult to test this theory in detail. Most graphite substrates have randomly oriented graphite planes and so the samples are two-dimensional powders from which the orientational order cannot be directly obtained. Single crystal graphite experiments are also not direct tests of the theory because the substrates then impose a sixfold substrate anisotropy. Nevertheless the results are in general accord with the predictions. Translationally disordered, but orientationally ordered hexatic phases, have been studied in detail [116] using thin films of liquid crystals and the experiments then very directly test the two-dimensional melting theory.

9.3. *Rotational epitaxy*

An important question in the growth of one material on another is the orientation of the two lattices. So far in this article we have always assumed that the directions of the high symmetry direction of the substrate and the layer are parallel. However, it was pointed out for rare gas monolayers on graphite that the monolayer might be rotated with respect to the orientation of the substrate [117] and soon afterwards a rotated phase was observed for argon on graphite [118].

The reason for the rotation is that in most materials it is less costly in energy to produce a shear distortion of the lattice than a compressive distortion; C_{11} is usually considerably larger than C_{44}. For the incommensurate phases discussed above, the average lattice constant of the layer is slightly larger or smaller than the substrate and so the energy of the commensuarate regions is controlled by the appropriate compressive elastic constant like C_{11}. If, however, the layer rotates slightly compared with substrate, the distortion produced by the substrate potential on the layer is a shear wave which is a less costly energy than the compressive wave. It is then energetically favourable for the monolayer to rotate with respect to the substrate. The angle of rotation is predicted [117] and found to vary approximately linearly with the lattice misfit. More complex theories have included the effects of anharmonicity and of nonlinear domain walls rather than harmonic phonons. The results [119, 120] not surprisingly then show that there is a critical misfit below which the layer and the substrate have the same orientation but beyond which the layer is

rotated with the transition being either continuous or of first order depending on the detailed parameters of the system.

§ 10. Incommensurate structures

Many materials have phases in which either the magnetic structure or crystallographic structure is modulated by a wave which is either incommensurate or has only a period which is very long compared with the lattice parameter of the underlying lattice [121]. Some long period alloy structures were found in Cu–Au alloys in the 1930s, while in the 1960s the rare earth metals were found to have incommensurately modulated magnetic structures and at much the same time ferroelectric materials such as $NaNO_2$ were found to have structurally incommensurate phases. The degree of incommensurability can usually be varied by varying the temperature, composition or an external field such as a magnetic field. The concepts used to describe these systems are very similar to those described above but the developments have taken place largely independently. In the next section we outline the continuum theory of these materials and then introduce the models which included the effects of the underlying lattice structure. In a final section we discuss some of the experimental results.

10.1. *Continuum theories of commensurate–incommensurate phase transitions*

The simplest model of a commensurate–incommensurate phase transition has already been discussed in section 9.1 and is the well known Frenkel–Kontorova model. For structurally incommensurate systems the kinetic energy term $(\mathrm{d}\phi/\mathrm{d}n - \delta)^2$ of equation (70) arises from a minimum in the phonon dispersion relation while the potential energy term V arises from the appropriate Umklapp terms in the potential energy and in this case a/a' is a small integer 3, 4 or 5. If $a/a' = 1$ or 2, the free energy has a different form because the dispersion relation is necessarily symmetric about the zone centre or the zone boundary, unlike wavevectors which are 1/3, 1/4 or 1/5 of a reciprocal lattice vector. In this latter case the theory is different [122] the commensurate–incommensurate transition is of first order and the transition cannot be studied in terms of an instability against the spontaneous creation of dislocations.

Returning to the cases with $a/a' = 3$, 4 or 5 the structure is commensurate if the energy to create a dislocation in the phase of the distortion, E_1, of equation (71), is positive. The structure is a modulated phase which minimizes the potential energy term. On changing the temperature the effective strength of the Umklapp terms may change so that the phase dislocation energy becomes negative leading to the spontaneous creation of dislocations, which have at times been called domain walls, solitons, or discommensurations. The theory predicts that the inverse spacing of the dislocations or, equivalently, the difference between the wavevector of the commensurate phase and the incommensurate phase varies as given by equation (74), namely $-\ln(\delta - \delta_c)$. This theory was originally developed for structural phase transitions by McMillan [104] and by Bak and Emery [29] and was given in more detail by Bruce *et al.* [122].

In section 9.1 the effect of fluctuations on this mean field argument was discussed for two-dimensional layers and it was shown that domain wall fluctuations then lead to an effective repulsive interaction between the domain walls and equation (74) becomes modified to a square root behaviour, equation (75). Fisher and Fisher [106]

have studied the effect of fluctuations in three dimensions and in agreement with Bruce *et al.* [122] have concluded that the effect of fluctuations is then negligible.

Equation (74) depends on the detailed nature of the interaction between the dislocations. The phase dislocations usually interact with the elastic strains so as to produce an effective attractive interaction between the phase dislocations. This is in contrast to the interaction between the elastic dislocations described in section 2 where their interaction may be of either sign. This interaction gives an additional term in the energy, equation (73), of the form $-1/p^2$ and the commensurate–incommensurate transition is then necessarily of first order.

Finally, the continuum model can be used to calculate the excitation spectrum of the incommensurate phase [123, 124]. The most notable feature is a branch with excitation frequencies proportional to wavevector corresponding to the acoustic modes of motion of the phase dislocation lattice. These modes are known as phasons and are Goldstone bosons associated with the broken phase symmetry of the incommensurate phase.

10.2. *Lattice models*

The continuum models described in the previous section result in an energy for the dislocations which is independent of the position of the centre of the dislocation in the unit cell. This is clearly incorrect unless the width of the core of the dislocation is much larger than a unit cell. A more realistic model should take account of the periodic variation of the energy within each unit cell. Much of the pioneering work on extending the Frenkel–Kontorova model to lattice models was performed by Aubry [125]. The analysis requires complex mathematics but the results can be understood qualitatively in a straightforward way. For the ground state at $T = 0$, the dislocations will be regularly arranged and situated at particular positions in the unit cell. These requirements give rise to long period commensurate structures having spacings between the dislocations which are an integer number of lattice parameters and which depend on the details of the model and experimentally on, say, external fields. Figure 25 shows a schematic calculation [126] of the reciprocal of the

Fig. 25

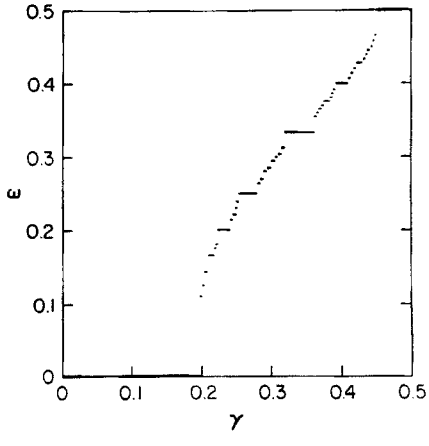

The wavevector or reciprocal average dislocation distance as a function of the misfit parameter γ [126].

Fig. 26

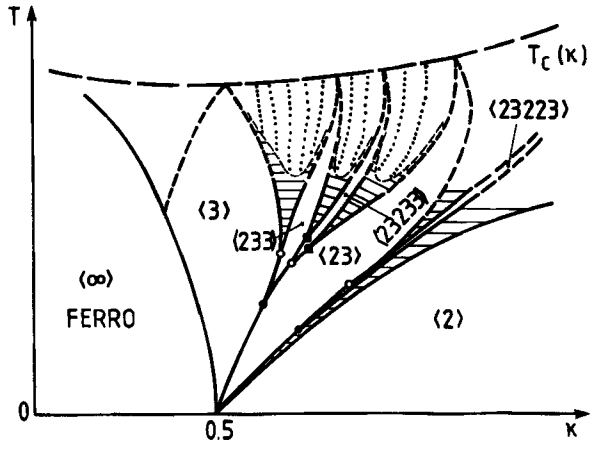

Possible phase diagram for the ANNNI model deduced from mean field theory [130]. At low T all phases are commensurate but above the dotted lines they are incommensurate.

average dislocation spacing $1/p_s$ or, alternatively, of the wavevector of the incommensurate state as the misfit parameter δ varies. Note that the envelope of the curve follows the logarithmic dependence of the continuum theory. States with particularly simple and regular arrangements of dislocations are the most stable in the sense that they occur over the widest intervals of γ. Sequences of solutions, such as those shown in figure 25, are known as Devil's staircases.

Similar models have been studied for magnetic systems with varying degrees of complexity to correspond to different real systems. One of the simplest is the ANNNI (axial-next-nearest-neighbour-Ising) model introduced by Elliott in 1961 to describe the modulated magnetic structure of erbium (for the early applications of the model see the review by Bak [127]; see also Fisher and Selke [128]). This model consists of ferromagnetically coupled sheets of Ising spins ($s = \frac{1}{2}$) but with the exchange interactions between nearest neighbour layers being J_1 and between next nearest layers, J_2. This model has been studied by many theoretical techniques: high and low temperature expansions, computer simulations and transfer matrix techniques [129]. At low temperatures these models also give commensurate long period phases and, for the ANNNI model, all these phases have the same energy when $J_2/J_1 = -0{\cdot}5$ as shown in figure 26 where the structure of the phases is indicated by the length of the ferromagnetic blocks. For example, the ⟨2333⟩ phase has ↑↑↓↓↑↑↑↓↓↓. As the temperature is raised the dislocations can move and there are completely incommensurate phases as well as commensurate ones and then, at the highest temperatures, the system becomes paramagnetic.

Although the particular details of the results are very dependent on the details of the models, this general picture is believed to be correct for the different models. At low temperatures the behaviour is dominated by long period commensurate phases with regularly spaced dislocations. At higher temperatures both long period commensurate and incommensurate phases occur because there is a sufficient entropy contribution to the free energy to overcome the localization energy of the lattice models. Nevertheless, in three-dimensional systems the dislocations are

undistorted and their spacing regular, unlike the melting described in section 9.1 for two-dimensional systems.

The systems described above have assumed that there is a unique direction and that the planes of the dislocations are perpendicular to that direction. In some real systems there are several equivalent directions, as occurs in TaS_2 which has three different but equivalent directions in the basal plane giving rise to the possibility of three different sets of domain walls which must then intersect one another. There has been comparatively little work done on these systems but Bak [130] argues that there will be an interaction energy due to the crossing of the domain walls and that this energy will depend on the number of crossings, namely $1/(p_1p_2)$, where p_1 and p_2 are the spacings of two different sets of dislocations. If the crossing energy is negative, the transition from a commensurate state to an incommensurate state is always of first order and the system forms an incommensurate phase with different sets of dislocations. If, on the other hand, the interaction is repulsive, the transition may be continuous but will be to an incommensurate phase with only one type of dislocation, known as a striped phase.

The analysis described above is for ideal pure crystals. In practice crystals always contain defects which can have the effect of pinning or partially pinning the phase dislocations. The largest effects occur for defects which produce random fields which locally favour the different ordered structures separated by the dislocation and so lead to fluctuations in the position of the dislocation. A dimensional argument then suggests that the fluctuations in position of a dislocation will increase with the linear size of dislocation L as $L^{2/3}$ in three dimensions [131]. This implies that the fluctuations diverge as L increases and that the dislocations necessarily interact in a similar way to the dislocations in two dimensions with thermal fluctuations as described in section 9. In the present case the energy of interaction due to these fluctuations is proportional to the separation, $1/p$, and so close to the phase transition for the spontaneous creation of dislocations the dislocation density increases as $(\delta - \delta_c)$ [131].

All of the results described in this section depend upon the establishment of thermodynamic equilibrium. Nevertheless the creation of dislocations at low temperatures and in the presence of imperfections may be inhibited by long relaxation times and indeed in comparing experimental results with theory for many systems the comparison is made difficult by these relaxation effects. As yet there has been far less work on the nucleation and blocking of these phase dislocations than that described for semiconductors in section 6.

10.3. *Experimental measurements*

In this section we review the evidence for dislocation like structures of incommensurate phases particularly close to commensurate phases. There are several different experimental techniques which have been used to provide evidence about dislocations.

(1) If the dislocations are well separated the neutron or X-ray scattering [132] consists of a series of sharp peaks with a definite relationship between the intensities of the primary peaks and the higher harmonics. Increasing the dislocation density alters the spacing of the peaks but not their intensities.

Fig. 27

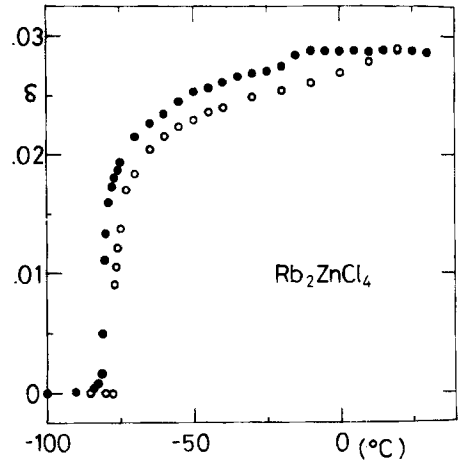

The temperature dependence of the modulation wavevector in Rb_2ZnCl_4. Full circles are cooling and open circles are heating [134].

(2) If the dislocations are well separated by commensurate regions, resonance techniques [133] will give sharp lines characteristic of the commensurate phase even in the incommensurate phase.
(3) Electron microscopy can be used to image the dislocations.

One of the most studied structural systems is that of Rb_2ZnCl_4 which below 303 K distorts to an incommensurate phase and then undergoes an incommensurate–commensurate transition at $T_c = 193$ K. The commensurate distortion is described by a wavevector along the $\mathbf{c}^*$ axis, $\mathbf{q} = (1/3 - \delta)\mathbf{c}^*$. Mashiyama *et al.* [134] made a detailed study of the temperature dependence of δ and their results are shown in figure 27. δ increases rapidly above T_c but there is a distinct difference between the results obtained on cooling and heating and pinning of the wavevector for $\delta = 0{\cdot}0288$. The difference in behaviour on heating and cooling suggests that the transition is of first order. Similar measurements on other incommensurate–commensurate transitions almost always give different results on heating and cooling, weakly first order transitions and pinning to wavevectors which depend on the history and defects present in the particular crystals.

Nevertheless these conclusions are broadly consistent with the theory discussed above in that the weakly first order transition is consistent with the effect of strains in producing an attractive force between the dislocations. The pinning illustrates the important effect of defects on the dislocations.

Andrews and Mashiyama [135] measured the X-ray scattering from the higher harmonics and found that even close to T_c their relative intensity was changing with temperature and that the satellites were much weaker than expected for well separated dislocations. This result suggests that the dislocation lattice may not be well defined even close to T_c.

NMR methods were used by Blinc *et al.* [136] to study Rb_2ZnCl_4 and provided evidence for commensurate lines in much of the incommensurate phase, as shown in figure 28. However, at T_c, they find that the soliton density is still 0·4 of the

Fig. 28

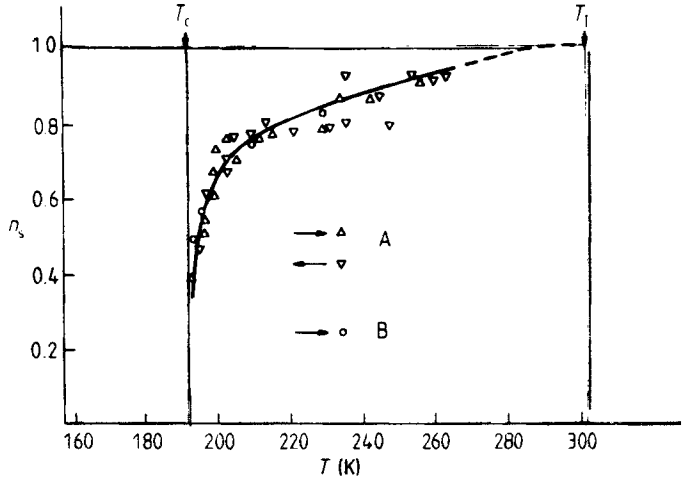

The temperature dependence of the dislocation density deduced from NMR measurements in Rb_2ZnCl_4 [133]. The units of n_s are normalized to be 1 at T_I.

maximum density which they ascribe to a chaotic dislocation phase due to defects. This seems a very high proportion of dislocations in the commensurate phase of a nominally pure crystal, for the dislocation lattice to be a good description.

Finally, Bestgen [136] has observed the incommensurate phase of Rb_2ZnCl_4 with electron microscopy and found lines whose spacing increased as $T \to T_c$ and interprets these lines as due to dislocations. Higher resolution images would enable us to identify if the dislocations are well defined or if they result from the imaging technique used for the incommensurate phase.

In conclusion there are indications that commensurate–incommensurate transitions can be described by phase dislocations but there is no system yet in which the continuum theory has been shown to be applicable and quantitatively correct.

Structural systems also show examples of long period commensurate structures particularly at low temperatures, or when a field is applied which favours particular commensurate phases. One example is thiourea which, in an applied electric field, has commensurate phases described by wavevectors of $1/9, 1/8, 2/15, 4/29, 6/43\mathbf{b}^*$ [137]. A simple physical model of thiourea has then developed to explain why these particular phases are the most stable. Many alloy systems also show long period commensurate phases and polytypism as reviewed by Yeomans [138] and these structures are examples of the behaviour which results when the dislocations interact with the crystal lattice as described in the previous section.

There are a number of magnetic systems whose magnetic structures also show incommensurate and long period magnetic structures. The rare earth metals are the best known examples and pure Ho and Er show examples of the effects. The crystal field anisotropy in Ho is such that the moments lie in the basal planes perpendicular to the hexagonal c-axis and within each plane the moments are aligned ferromagnetically. The moment does, however, rotate from one plane to the next to give a helical magnetic structure described by a wavevector, $\mathbf{q}_I$. On cooling below 133 K, the wavevector $\mathbf{q}_I$ is incommensurate $\approx \frac{2}{7}\mathbf{c}^*$ and on further cooling $\mathbf{q}_I$ decreases until

Fig. 29

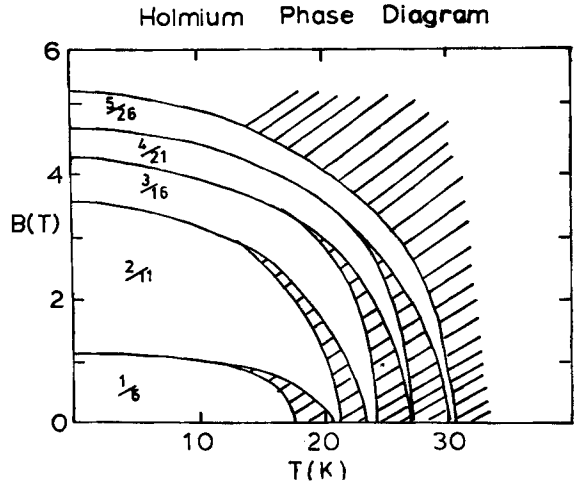

The magnetic phase diagram of holmium when the magnetic field is applied along the *c*-axis [142]. The fractions give the primary wavevector of the commensurate phases and the hatched region corresponds to incommensurate phases.

it locks into the commensurate wavevector at about 18 K with $\mathbf{q}_I = \frac{1}{6}\mathbf{c}^*$. The transition to the commensurate phase is however of first order and shows considerable hysteresis. The commensurate phase enables the structure to take advantage of the crystal field energy within the basal plane by having two successive planes closely aligned to each easy direction in the basal plane.

One of the first magnetic X-ray scattering experiments with synchrotrons was performed on Ho and showed that just above 18 K there were a number of long period commensurate phases [139]. It was suggested that these arose because of regular dislocations in the commensurate structure, with particular easy axes being associated with only one basal plane. Neutron scattering measurements [140] were then performed which showed that the higher harmonics of the scattering could be accounted for by this model confirming that the dislocation model is a good model of these phases. Similar results [141] have now been obtained for the long period magnetic phases of erbium.

The phase diagrams of a number of magnetic systems also show many commensurate phases. An example is shown in figure 29 for holmium when a magnetic field is applied along the *c*-axis. At low temperatures when entropy effects are minimized only commensurate phases occur but at higher temperatures there are also incommensurate phases [142]. CeSb is another material which shows many long period structures but in this case the phase diagram shows only long period commensurate phases [143].

§ 11. Conclusions

This review has been concerned with a class of phase transitions which are associated with the spontaneous creation of dislocations in condensed matter. These are different from most phase transitions because at the latter the changes at the phase transition are distributed fairly uniformly throughout the material whereas in

these phase transitions there are large distortions at the cores of the dislocations and much smaller ones between the dislocations. Much of the review has been concerned with a detailed description of the theory and experiment for thin films of semiconductors grown on top of suitable substrates. This is important for technology because the dislocations spoil the electrical properties of the layers and so the semiconducting films must be sufficiently thin that no dislocations are produced. Much of the emphasis in this field has therefore been on calculating the film thickness at which the transition occurs, h_c.

We show, however, that the same ideas are also used to describe a number of other systems: the structure of epitaxial films on graphite and commensurate–incommensurate transitions in both structural and magnetic systems. In these cases the motivation has often been to study the statistical mechanics and so theory and experiment have concentrated on the critical behaviour close to the transition. Nevertheless, it is clear that similar problems have arisen in the different fields.

As the dislocations become further apart the forces become very weak and so these phase transitions are very subtly dependent on the forces between the dislocations and also on any defects or lattice structure which can pin the dislocations. In almost all fields there has been discussion and controversy about the nature of the forces between the dislocations. The simplest argument is that the interaction falls off with the distance between the dislocations as $\exp(-p/\lambda)$. This, however, must be modified by the interaction of the dislocations with the strain in the lattice and this decreases as $1/p^2$ and so is the dominant interaction at large distances. Furthermore this interaction is often, but not always, attractive and so is probably responsible for the transition being of first order.

If the dislocations are not flat but can wander then they will interact with one another by confining the space within which each can wander. This leads to an entropic interaction and for two-dimensional systems this leads to a repulsive interaction due to the thermal fluctuations which is repulsive and proportional to $1/p^2$. There is good experimental evidence for this. In three dimensions the thermal fluctuations do not give rise to this wandering but defects can produce similar effects except that the interaction may be repulsive and of the form $1/p$. There is no clear evidence for this type of behaviour. Clearly the nature of the interaction between the dislocations is a complex problem but one which has crucial consequences.

In the theory of commensurate–incommensurate transitions the role of the lattice or crystal field pinning of the dislocations is important. If this pinning energy is small then genuinely incommensurate phases occur at high temperatures but the systems tend to have long period commensurate structures at low temperatures. There seems to have been little discussion of the effects of lattice pinning for semiconductors but possibly this is because the results of the theory are of technological interest only when the distance between the dislocations is many lattice constants.

There has also been relatively little effort to understand systems where there are different intersecting sets of dislocations or where the film has a lattice rotated from the principal axes of the substrate. Both of these effects can drastically alter the behaviour of the materials and more work is needed to understand the different properties.

Finally, because dislocations are localized they inevitably are pinned by defects and so the properties of real systems are strongly influenced by defects and imperfections. The problems of establishing thermodynamic equilibrium then lead to long time constants, irreversibility and metastability. It is well known that all these

occur but as yet relatively little has been done to understand the effects quantitatively.

We hope that this review will have described the present situation in understanding the critical thickness of Ge_xSi_{1-x} layers and then have shown that the theory is also applicable to many other systems. Perhaps the results obtained in one aspect of the understanding of dislocation structures will lead to advances in other areas.

ACKNOWLEDGMENTS

We are grateful for helpful discussions with A. D. Bruce. Financial support in Oxford was provided by the Engineering and Physical Sciences Research Council.

REFERENCES

[1] JAIN, S. C., and HAYES, W., 1991, *Semicond. Sci. Technol.*, **6**, 547.
[2] SZE, S. M. (editor), 1990, *High Speed Semiconductor Devices* (New York: Wiley Interscience).
[3] MORGAN, D. V., and WILLIAMS, R. H. (editors), 1991, *Physics and Technology of Semiconductor Heterojunction Devices* (London: Peregrinus).
[4] KASPER, E., and SCHÄFFLER, F., 1991, *Semiconductors and Semimetals*, Vol. 33, edited by T. P. Pearsall (London: Academic Press), pp. 223–309.
[5] JAIN, S. C., 1994, *Germanium–Silicon Strained Layers and Heterostructures* (Boston: Academic Press).
[6] FU, Y., JAIN, S. C., WILLANDER, M., and LOFERSKI, J. J., 1993, *J. appl. Phys.*, **74**, 402.
[7] JAIN, S. C., IYER, S. S., and LOFERSKI, J. J., 1992, *AVS Topical Conference*, 9–13 November, Chicago, poster paper.
[8] JAIN, S. C., POORTMANS, J., IYER, S. S., LOFERSKI, J. J., NIJS, J., MERTENS, R., and VAN OVERSTRAETEN, R., 1993, *IEEE Trans. Electron. Devices*, **40**, 2338.
[9] BEAN, J. C., 1992, *Proc. IEEE*, **80**, 571.
[10] PEOPLE, R., 1986, *IEEE J. Quantum Electron.*, **QE 22**, 1696. See also PEOPLE, R., and BEAN, J. C., 1986, *Appl. Phys. Lett.*, **48**, 1338.
[11] SCHÄFFLER, F., TÖBBEN, D., HERZOG, H.-J., ABSTREITER, G., and HOLLÄNDER, B., 1992, *Semicond. Sci. Technol.*, **7**, 260.
[12] PATTON, G. L., COMFORT, J. H., MEYERSON, B. S., CRABBÉ, E. F., SCILLA, G. J., DE FRESART, E., STORK, J. M. C., SUN, J. Y. C., HARAME, D. L., and BURGHARTZ, J. N., 1990, *IEEE Electron. Device Lett.*, **11**, 171.
[13] GRUHLE, A., KIBBEL, H., ERBEN, U. and KASPER, E., 1993, *Electron. Lett.*, **29**, 415.
[14] TSAUR, B.-Y., CHEN, C. K., and MARINO, S. A., 1991, *IEEE Electron. Device Lett.*, **12**, 293.
[15] GARONE, P. M., VENKATARAMAN, V., and STURM, J. C., 1992, *IEEE Electron. Device Lett.*, **13**, 56.
[16] OSBOURN, G. C., 1986, *IEEE J. Quantum Electron.*, **QE-22**, 1677.
[17] ADACHI, S., 1992, *Physical Properties of III–V Semiconductor Compounds* (New York: Wiley).
[18] ADAMS, A., and O'REILLY, E., 1992, *Phys. World*, **5** (October), 43.
[19] YORK, P. K., BEERNINK, K. J., FERNANDEZ, G. E., and COLEMAN, J. J., 1990, *Semicond. Sci. Technol.*, **5**, 508.
[20] CHAND, N., BECKER, E. E., VAN DER ZIEL, J. P., CHU, S. N. G., and DUTTA, N. K., 1991, *Appl. Phys. Lett.*, **58**, 1704.
[21] MORKOC, H., SVERDLOV, B., and GAO, G.-B., 1993, *Proc. IEEE*, **81**, 493.
[22] GUNSHOR, R. L., OTSUKA, N., and NURMIKKO, A. V., 1993, *IEEE Spectrum*, **30**, 28.
[23] HASSE, M. A., QUI, J., DEPUYDT, J. M., and CHENG, H., 1991, *Appl. Phys. Lett.*, **57**, 1272.
[24] REN, J., BOWERS, K., SHEED, B., DREIFUS, D. L., COOK, JR, J. W., SCHETSINA, J. F., and KOLBAS, R. M., 1990, *Appl. Phys. Lett.*, **57**, 1901.
[25] JEON, H., DING, J., PATTERSON, W., NURMIKO, A. V., XIE, W., GRILLO, D. C., KOBAYASHI, M., and GUNSHOR, R. L., 1991, *Appl. Phys. Lett.*, **59**, 3619.

[26] GLASS, A. M., TAI, K., BYLSMA, R. B., FELDMAN, R. D., OLSON, D. H., and AUSTIN, R. F., 1988, *Appl. Phys. Lett.*, **53,** 834.
[27] BAIBICH, M. N., BROTO, J. M., FERT, A., NGUYEN VAN DAU, F., PETROFF, F., ETIENNE, P., CREUZET, G., FRIEDERICH, A., and CHAZELAS, J., 1988, *Phys. Rev. Lett.*, **61,** 2472.
[28] BARNETT, S. A., 1993, *Physics in Thin Films*, edited by M. H. Francombe and J. L. Vossen (New York: Academic Press), chapter 1.
[29] BAK, P., and EMERY, V. J., 1976, *Phys. Rev. Lett.*, **36,** 978.
[30] SHOCKLEY, W., 25 September 1951, US Patent 2569347.
[31] KROEMER, H., 1957, *Proc. IRE*, **45,** 1535.
[32] KROEMER, H., 1982, *Proc. IEEE*, **70,** 13.
[33] TIWARI, A., and FRANK, D. J., 1992, *Appl. Phys. Lett.*, **60,** 630.
[34] SHUR, M., 1990, *Physics of Semiconductor Devices* (Englewood Cliffs, NJ: Prentice Hall), pp. 632–633.
[35] FRANK, F. C., and VAN DER MERWE, J., 1949, *Proc. R. Soc. (Lond.)*, **A 198,** 216.
[36] BALL, C. A. B., and VAN DER MERWE, J. H., 1983, *Dislocations in Solids*, edited by F. R. N. Nabarro (Amsterdam: North Holland), chapter 27, pp. 122–141.
[37] NAGAI, H., 1974, *J. appl. Phys.*, **45,** 3789.
[38] KASPER, E., HERZOG, H. J., and KIBBEL, H., 1975, *Appl. Phys.*, **8,** 199.
[39] KASPER, E., and HERZOG, H. J., 1977, *Thin Solid Films*, **44,** 357.
[40] JAIN, S. C., BULLOUGH, R., and WILLIS, J., 1990, *Adv. Phys.*, **39,** 127.
[41] MATTHEWS, J. W., 1975, *Epitaxial Growth*, Part B, edited by J. W. Matthews (New York: Academic Press), pp. 559–609.
[42] MATTHEWS, J. W., 1975, *J. Vac. Sci. Technol.*, **12,** 126.
[43] JAIN, S. C., 1989, *Proceedings of the Fifth International Workshop on the Physics of Semiconductor Devices*, edited by W. S. Khokle and S. C. Jain (Delhi: Macmillan), pp. 3–12.
[44] JAIN, S. C., GOSLING, T. J., WILLIS, J. R., TOTTERDELL, D. H. J., and BULLOUGH, R., 1992, *Phil. Mag.* A, **65,** 1151.
[45] JAIN, U., JAIN, S. C., NIJS, J., WILLIS, J. R., BULLOUGH, R., MERTENS, R., and VAN OVERSTRAETEN, R., 1993, *Solid-State Electron.*, **36,** 331.
[46] WILLIS, J. R., JAIN, S. C., and BULLOUGH, R., 1990, *Phil. Mag.* A, **62,** 115.
[47] LEGOUES, F. K., HORN-VON HOEGEN, M., COPEL, M., and TROMP, R. M., 1991, *Phys. Rev.* B, **44,** 12 894.
[48] PRICE, G. L., 1991, *Phys. Rev. Lett.*, **66,** 469.
[49] JAIN, S. C., GOSLING, T. J., WILLIS, J. R., BULLOUGH, R., and BALK, P., 1992, *Solid-State Electron.*, **35,** 1073.
[50] WILLIS, J. R., JAIN, S. C., and BULLOUGH, R., 1991, *Phil. Mag.* A, **64,** 629.
[51] GOSLING, T. J., BULLOUGH, R., JAIN, S. C., and WILLIS, J. R., 1993, *J. appl. Phys.*, **73,** 8267.
[52] ATKINSON, A., and JAIN, S. C., 1992, *J. appl. Phys.*, **72,** 2242.
[53] ATKINSON, A., and JAIN, S. C., 1992, *Thin Solid Films*, **222,** 161.
[54] ATKINSON, A., and JAIN, S. C., 1993, *J. Phys.: condens. Matter*, **5,** 4595.
[55] JAIN, U., JAIN, S. C., ATKINSON, A., NIJS, J., MERTENS, R., and VAN OVERSTRAETEN, R., 1993, *J. appl. Phys.*, **73,** 1773.
[56] ROCKETT, A., and KIELY, C. J., 1991, *Phys. Rev.* B, **44,** 1154.
[57] FRITZ, I. J., 1987, *Appl. Phys. Lett.*, **51,** 1080.
[58] FRITZ, I. J., 1987, *Appl. Phys. Lett.*, **51,** 1004.
[59] HOUGHTON, D. C., GIBBINGS, C. J., TUPPEN, C. G., LYONS, M. H., and HALLIWELL, M. A. G., 1990, *Appl. Phys. Lett.*, **56,** 460.
[60] HOUGHTON, D. C., GIBBINGS, C. J., TUPPEN, C. G., LYONS, M. H., and HALLIWELL, M. A. G., 1989, *Thin Solid Films*, **183,** 171.
[61] ANDERSSON, T. G., CHEN, Z. G., KULAKOVSKII, V. D., UDDIN, A., and VALLIN, J. T., 1987, *Appl. Phys. Lett.*, **51,** 752.
[62] MATTHEWS, J. W., and BLAKESLEE, A. E., 1974, *J. Cryst. Growth*, **27,** 118.
[63] JAIN, S. C., BALK, P., GOORSKY, M. S., and IYER, S. S., 1991, *Microelectron. Engng*, **15,** 131.

[64] PAYNE, A. P., NIX, W. D., LAIRSON, B. M., and CLEMENS, B. M., 1993, *Phys. Rev.*, **47**, 13 730.
[65] EAGLESHAM, D. J., GOSSMANN, H.-J., and CERULLO, M., 1990, *Mater. Res. Soc. Symp. Proc.*, Vol. 198 (Pittsburgh, Pennsylvania: Materials Research Society), pp. 51–56.
[66] WILLIAMS, A. A., THORNTON, J. M. C., MACDONALD, J. E., VAN SILFHOUT, R. G., VAN DER VEEN, J. F., FINNEY, M. S., JOHNSON, A. D., and NORRIS, C., 1991, *Phys. Rev.* B, **43**, 5001.
[67] HOUGHTON, D. C., 1991, *J. appl. Phys.*, **70**, 2136.
[68] TUPPEN, C. G., and GIBBINGS, C. J., 1990, *J. appl. Phys.*, **68**, 1526.
[69] HULL, R., BEAN, J. C., BAHNCK, D., PETICOLAS, JR, L. J., SHORT, K. T., and UNTERWALD, F. C., 1991, *J. appl. Phys.*, **70**, 2052.
[70] HULL, R., and BEAN, J. C., 1989, *J. Vac. Sci. Technol.* A, **7**, 2580.
[71] EAGLESHAM, D. J., KVAM, E. P., MAHER, D. M., HUMPHREYS, C. J., and BEAN, J. C., 1989, *Phil. Mag.* A, **59**, 1059.
[72] GOSLING, T. J., JAIN, S. C., and HARKER, A. H., 1994, *Phys. Stat. sol.* (a), **146**, 713.
[73] DODSON, B. W., 1988, *Heteroepitaxy on Silicon: Fundamentals, Structure and Devices*, Vol. 116, edited by H. K. Choi, R. Hull, H. Ishiwara and R. H. Nemanich (Pittsburgh, Pennsylvania: Materials Research Society), pp. 491–503.
[74] HOUGHTON, D. C., 1990, *Appl. Phys. Lett.*, **57**, 1434.
[75] HOUGHTON, D. C., 1990, *Appl. Phys. Lett.*, **57**, 2124.
[76] FREUND, L. B., and HULL, R., 1992, *J. appl. Phys.*, **71**, 2054.
[77] HIRTH, J. P., and LOTHE, J., 1968, *Theory of Dislocations* (New York: McGraw-Hill).
[78] LOUCHET, F., COCHET MUCHY, D., and BRECHET, Y., 1988, *Phil. Mag.* A, **57**, 327.
[79] LOUCHET, F., 1981, Institute of Physics Conference Series, No. 60 (Bristol: Institute of Physics), pp. 35–38.
[80] SUMINO, K., and YONENAGA, I., 1991, *Solid State Phenomena*, **19–20**, 295.
[81] BONAR, J. M., HULL, R., WALKER, J. F., and MALIK, R., 1992, *Appl. Phys. Lett.*, **60**, 13 279.
[82] PAINE, D., HOWARD, D. J., SACKS, D. R. N., and ESCHRICH, T. C., 1990, *Mater. Res. Soc. Symp. Proc.*, Vol. 160 (Pittsburgh, Pennsylvania: Materials Research Society), pp. 123–128.
[83] PEROVIC, D. D., and HOUGHTON, D. C., 1992, *Mechanisms of Heteroepitaxial Growth*, Mater. Res. Soc. Symp. Proc., Vol. 263, edited by M. F. Chisholm, B. J. Garrison, R. Hull and L. J. Schowalter, (Pittsburgh, Pennsylvania: Materials Research Society), pp. 391–402.
[84] FITZGERALD, E. A., WATSON, G. P., PROANO, R. E., and AST, D. G., 1989, *J. appl. Phys.*, **65**, 2220.
[85] TUPPEN, C. G., GIBBINGS, C. J., HOCKLY, M., and ROBERTS, S. G., 1990, *Appl. Phys. Lett.*, **56**, 54.
[86] HIGGS, V., KIGHTLEY, P., GOODHEW, P. J., and AUGUSTUS, P. D., 1991, *Appl. Phys. Lett.*, **59**, 829.
[87] HULL, R., BEAN, J. C., BAHNCK, D., BONAR, J. M., and PETICOLAS, L. J., 1991, *Proceedings of the Microscopy and Semiconductor Materials Conference*, Institute of Physics Conference Series No. 117 (Bristol: Institute of Physics), pp. 497–508.
[88] HULL, R., BEAN, J. C., and BUESCHER, C., 1989, *J. appl. Phys.*, **66**, 5837.
[89] LEGOUES, F. K., MOONEY, P. M., and CHU, J. O., 1993, *Appl. Phys. Lett.*, **62**, 140.
[90] NIX, W. D., NOBLE, D. B., and TURLO, J. F., 1990, Mechanism and kinetics of misfit dislocation formation in heteroepitaxial thin films. *Materials Research Society 1990 Spring Meeting*, 16–21 April, San Francisco, California (Pittsburgh, Pennsylvania: Materials Research Society).
[91] LEGOUES, F. K., OTT, J. A., EBERL, K., and IYER, S. S., 1992, *Appl. Phys. Lett.*, **61**, 174.
[92] (a) KAMAT, S. V., and HIRTH, J. P., 1990, *J. appl. Phys.*, **67**, 6844. (b) HAGEN, W., and STRUNK, H., 1978, *Appl. Phys.*, **17**, 85.
[93] LEFEBVRE, A., HERBEAUX, C., BOUILLET, C., and DI PERSIO, J., 1991, *Phil. Mag. Lett.*, **63**, 23.
[94] FREUND, L. B., 1990, *J. appl. Phys.*, **68**, 2073.
[95] ALEXANDER, H., and HAASAN, P., 1968, *Solid State Physics*, Vol. 22, edited by F. Seitz, D. Turnbull, and H. Ehrenreich (New York: Academic Press), pp. 27–158.

[96] BEAN, J. C., FELDMAN, L. C., FIORY, A. T., NAKAHARA, S., and ROBINSON, I. K., 1984, *J. Vac. Sci. Technol.*, **A2,** 436.
[97] JESSER, W. A., and MATTHEWS, J. W., 1968, *Phil. Mag.*, **17,** 461.
[98] FARTOSH, A., GRIMSDITCH, M., FULLERTON, E. E., and SCHULLER, I. K., 1993, *Phys. Rev.* B, **47,** 12 813, and references therein.
[99] SONNTAG, P., DONNER, W., METOKI, N., and ZABEL, H., 1994, *Phys. Rev.* B, **49,** 2869.
[100] SPECK, J. S., and POMPE, W., 1994, *J. appl. Phys.*, **76,** 466.
[101] SPECK, J. S., SEIFERT, A., POMPE, W., and RAMESH, R., 1994, *J. appl. Phys.*, **76,** 477.
[102] POMPE, W., GONG, X., SUO, Z., and SPECK, J. S., 1993, *J. appl. Phys.*, **74,** 6012.
[103] MOCHRIE, S. G. J., GIBBS, D., and ZEHNER, D. M., 1992, *Materials Interfaces: Atomic-Level Structure and Properties*, edited by D. Wolf and S. Yip (London: Chapman and Hall), p. 336.
[104] MCMILLAN, W. L., 1976, *Phys. Rev.* B, **14,** 1496.
[105] POKROVSKY, V. L., and TALAPOV, A. L., 1979, *Phys. Rev. Lett.*, **42,** 65.
[106] FISHER, M. E., and FISHER, D. S., 1982, *Phys. Rev.* B, **25,** 3192.
[107] ERBIL, A., KORTAN, A. R., BIRGENEAU, R. J., and DRESSELHAUS, M. S., 1983, *Phys. Rev.* B, **28,** 6329.
[108] MOCHRIE, S. G. J., KORTAN, A. R., BIRGENEAU, R. J., and HORN, P. M., 1985, *Z. Phys.* B, **62,** 79.
[109] STEPHENS, P. W., HEINEY, P., BIRGENEAU, R. J., and HORN, P. M., 1979, *Phys. Rev. Lett.*, **43,** 47.
[110] STEPHENS, P. W., HEINEY, P. A., BIRGENEAU, R. J., HORN, P. M., MONCTON, D. E., and BROWN, G. S., 1984, *Phys. Rev.* B, **29,** 3512.
[111] COPPERSMITH, S. N., FISHER, D. S., HALPERIN, B. I., LEE, P. A., and BRINKMAN, W. F., 1982, *Phys. Rev.* B, **25,** 349.
[112] KOSTERLITZ, J. M., and THOULESS, D. J., 1972, *J. Phys.* C, **5,** L124.
[113] NELSON, D. R., 1978, *Phys. Rev.* B, **18,** 2318.
[114] NELSON, D. R., and HALPERIN, B. I., 1979, *Phys. Rev.* B, **19,** 2457.
[115] HEINEY, P. A., STEPHENS, P. W., BIRGENEAU, R. J., HORN, P. M., and MONCTON, D. E., 1983, *Phys. Rev.* B, **28,** 6416.
[116] PINDAK, R., MONCTON, D. E., DAVEY, S. C., and GOODBY, J. W., 1981, *Phys. Rev. Lett.*, **46,** 1135.
[117] NOVACO, A. D., and MCTAGUE, J. P., 1977, *Phys. Rev. Lett.*, **38,** 1286.
[118] SHAW, C. G., FAIN, JR, S. C., and CHINN, M. D., 1978, *Phys. Rev. Lett.*, **41,** 955.
[119] SHIBA, H., 1979, *J. Phys. Soc. Japan*, **46,** 1852.
[120] SHIBA, H., 1980, *J. Phys. Soc. Japan*, **48,** 211.
[121] For a review see BLINC, R., and LEVANYUK, A. P., 1986, *Incommensurate Phases in Dielectrics*, Vol. 1 and 2 (Amsterdam: North Holland).
[122] BRUCE, A. D., COWLEY, R. A., and MURRAY, A. F., 1978, *J. Phys.* C, **11,** 3591.
[123] BRUCE, A. D., and COWLEY, R. A., 1978, *J. Phys.* C, **11,** 3609.
[124] POKROVSKII, V. L., and TALAPOV, A. L., 1978, *Sov. Phys. JETP*, **48,** 579 (1978, *Zh. Eksp. Teor. Fiz.*, **75,** 1151).
[125] AUBRY, S., 1983, *J. Phys.* C **16,** 2497.
[126] CHOU, W., and GRIFFITHS, R. B., 1986, *Phys. Rev.* B, **34,** 6219.
[127] BAK, P., 1982, *Rep. Progr. Phys.*, **45,** 587.
[128] FISHER, M. E., and SELKE, W., 1980, *Phys. Rev. Lett.*, **44,** 1502.
[129] SELKE, W., 1992, Spatially modulated structures in systems with competing interactions. *Phase Transitions and Critical Phenomena*, Vol. 15, edited by C. Domb and J. L. Lebowitz (New York: Academic).
[130] BAK, P., 1979, *Solitons and Condensed Matter Physics, Proceedings of the Symposium on Nonlinear (Soliton) Structure and Dynamics in Condensed Matter*, Oxford, 22–28 June 1978, edited by A. R. Bishop and T. Schneider (Berlin: Springer), p. 216.
[131] NATTERMANN, T., 1983, *J. Phys.* C, **16,** 4125.
[132] COWLEY, R. A., 1980, *Adv. Phys.*, **29,** 1.
[133] BLINC, R., RUTAR, V., TOPIĆ, B., ŽUMER, S., SELIGER, I. P., ALEKSANDROVA, I. P., and MILIA, F., 1986, *J. Phys.* C, **19,** 3421.
[134] MASHIYAMA, J., TANISAKI, S., and HAMANO, K., 1982, *J. Phys. Soc. Japan*, **51,** 2538.
[135] ANDREWS, S. R., and MASHIYAMA, H., 1983, *J. Phys.* C, **16,** 4985.

[136] BESTGEN, H., 1986, *Solid State Commun.*, **58,** 197.
[137] MOUDDEN, A. H., MONCTON, D. E., and AXE, J. D., 1980, *Phys. Rev. Lett.*, **51,** 2390.
[138] YEOMANS, J., 1988, *Solid State Physics*, Vol. 41, edited by F. Seitz, D. Turnbull, and H. Ehrenreich (New York: Academic Press), p. 151.
[139] GIBBS, D., MONCTON, D. E., D'AMICO, K. L., BOHR, J., and GRIER, B. H., 1985, *Phys. Rev. Lett.*, **55,** 234.
[140] COWLEY, R. A., and BATES, S., 1988, *J. Phys.* C, **21,** 4113.
[141] COWLEY, R. A., and JENSEN, J., 1992, *J. Phys.: condens. Mater.*, **4,** 9673.
[142] COWLEY, R. A., JEHAN, D. A., MCMORROW, D. F., and MCINTYRE, G. J., 1991, *Phys. Rev. Lett.*, **66,** 1521.
[143] ROSSAT-MIGNOD, J., BURLET, P., BARTHOLIN, H., VOGT, O., and LAGNIER, R., 1980, *J. Phys.* C, **13,** 6381.